

# Streamwise oscillations of a cylinder in steady current. Part 2. Free-surface effects on vortex formation and loading

By O. CETINER<sup>†</sup> AND D. ROCKWELL

Department of Mechanical Engineering and Mechanics, 354 Packard Laboratory,  
19 Memorial Drive West, Lehigh University, Bethlehem, PA 18015, USA

(Received 22 April 1999 and in revised form 24 July 2000)

A cylinder in a steady current beneath a free surface is subjected to oscillations in the streamwise direction. Techniques of high-image-density particle image velocimetry and instantaneous force measurement provide the relationship between the instantaneous, global flow patterns and the unsteady loading on the cylinder.

The existence of locked-on states for the fully submerged cylinder is addressed in the companion study of Cetiner & Rockwell (2001). The present investigation shows that it is possible to generate distinctly different locked-on states of vortex formation, provided the cylinder is located immediately beneath the free surface. As a consequence, the time-dependent transverse force is phase-locked to the cylinder motion. In the event that a finite gap exists between the cylinder and the free surface, however, instantaneous, jet-like flow through the gap acts to destabilize such locked-on states. Lissajous representations of the forces demonstrate the degree of phase-locking or, in some cases, a loss of lock-on and associated phase drift. Moreover, the degree of submergence of the cylinder beneath the free surface has remarkable consequences for the magnitudes of positive and negative spikes of the time-dependent force signatures, as well as the averaged spectra of the transverse force. In turn, these alterations of the unsteady transverse force are accompanied by substantial changes of the averaged in-line and transverse forces.

Vortex systems can exist at locations both upstream and downstream of the cylinder. They are due to vorticity from the cylinder surface and/or the free surface. The space–time development of the entire system of vorticity concentrations is interpreted in terms of the time histories of the relative velocity of the cylinder and the instantaneous forces on the cylinder. In turn, these features of the vorticity field are related to critical points near the free surface, deduced from topologies of the corresponding velocity and streamline patterns. Despite the fact that changes in the patterns of vorticity and the corresponding topologies occur in conjunction with large fluctuations of the transverse force coefficient, the dimensionless strength of the vortices is below the threshold for which distinguishable, localized deformations of the free surface occur.

---

## 1. Introduction

Combined wave motion and steady current past ocean structures can induce severe loading and vibration. Representative structures having a cylindrical geometry include towing cables, which may be inclined at an angle with respect to the free surface;

<sup>†</sup> Present address: Istanbul Technical University, Turkey.

in some cases, they may be at a shallow angle with respect to the free surface, thereby approximating a horizontal orientation. Rapidly deployable cable systems with instrumentation can be dropped from an aircraft through a free surface and, during the initial stages of deployment, may be oriented horizontally beneath the free surface. Moreover, offshore platforms typically have horizontal, cylindrically shaped members. The essential features of wave-current loading of all of these configurations can be approximated by a horizontal cylinder in proximity to a free surface. Furthermore, it should be noted that various configurations of mines and other submerged obstacles, though having a spherical or other non-cylindrical shape, can be deployed at or immediately beneath a free surface. Certain of the features of the loading and wave-current patterns past the upper surface of such bodies are expected to be generic to both cylindrical and non-cylindrical configurations.

Wave loading of cylinders, in the absence of steady current, has been investigated experimentally in a variety of systems, including wave tanks and U-tube tunnels. The latter type of system involves generation of unidirectional, harmonic motion past a stationary cylinder, thereby simulating the loading due to infinitely long waves. Representative investigations in this category include those of Sarpkaya (1975) and Obasaju, Bearman & Graham (1988). Alternatively, the loading due to long-wave motion can be characterized by unidirectional oscillations of the cylinder in quiescent water, provided that the Froude-Krylov force is accounted for (Lighthill 1986). A representative investigation using this approach is that of Williamson (1985). All of these studies of unidirectional wave motion past a cylinder, including the references cited therein, have centred on the case of a fully submerged cylinder, i.e. a cylinder in the absence of free-surface effects.

The present investigation addresses the case of unidirectional oscillations of a horizontal cylinder located beneath a free surface. The intent is to determine the consequence of proximity to the free surface on the instantaneous and averaged loading, which will be interpreted in conjunction with patterns of instantaneous velocity, vorticity and streamline topology. These features will be compared with the corresponding case of a fully submerged, unidirectionally oscillating cylinder, described in the companion study of Cetiner & Rockwell (2001). In the following, relevant investigations of loading of cylinders in proximity to a free surface are described; they have focused on the limiting cases of steady translation of the cylinder beneath the free surface or steady flow past a stationary cylinder. Then, oscillatory wave motion past a stationary cylinder and oscillation of a cylinder in quiescent fluid are addressed for the case of an adjacent free surface, but in the absence of a steady current. Finally, the case of a transversely oscillating cylinder at a free surface in the absence of steady current is discussed. These investigations of vortex generation and loading in the presence of a free surface give useful information and provide quantitative characterization of the instantaneous vorticity fields, via either quantitative experimental images or numerical calculations.

The limiting case of translation of a cylinder at constant velocity through quiescent fluid in the presence of an adjacent free surface was addressed by Miyata, Shikazono & Kanai (1990). In their investigation, the effective Froude number was sufficiently small, so the free surface exhibited negligible distortion. Using a combination of qualitative flow visualization, force measurements and numerical simulation, they related patterns of vortices to the forces on the cylinder. Sheridan, Lin & Rockwell (1997) considered the case of steady incident flow past a cylinder close to a free surface. They quantitatively characterized the patterns of velocity and vorticity for higher values of Froude number. Distortion of the free surface led to generation of

vorticity layers and concentrations not only from the surface of the cylinder, but from the free surface as well. The interplay between these two origins of vorticity leads to several classes of near-wake structure that undoubtedly have important implications for the loading on the cylinder.

For the case where the cylinder undergoes simultaneous steady translation and a prescribed vertical acceleration beneath the free surface, Zhu *et al.* (2000) demonstrate that the timing of vortex formation from the upper surface of the cylinder, relative to that from the lower surface, is dramatically altered when the gap between the free surface and the cylinder is varied. The altered patterns of streamline topology and vorticity provide a physical basis for interpreting the substantial changes in the instantaneous in-line and transverse force coefficients.

In the event that a surface-piercing cylinder is subjected to vertical (periodic) acceleration in the presence of a steady current, Lin, Sheridan & Rockwell (1996) show that the near wake of the cylinder exhibits pronounced concentrations of vorticity from the lower surface, in conjunction with a relatively long reattachment length of the separated shear layer to the surface. This pattern could, however, be altered substantially when the cylinder was subjected to vertical oscillations at or near the frequency corresponding to inherent vortex formation from the lower surface of the cylinder.

In-line oscillations of a cylinder beneath a free surface have received less attention; the case of simultaneous steady current and in-line oscillations has not been addressed. Lin & Rockwell (1999) considered the limiting case of harmonic, in-line oscillations of a cylinder in quiescent fluid and demonstrated the relationship between the instantaneous patterns of vorticity and the instantaneous signatures of the transverse force. In the extreme case where the cylinder is located sufficiently close to the free surface such that no gap exists, the patterns of vorticity are highly repetitive and, unlike cases of deeper submergence beneath the free surface, a principal contribution to pronounced negative spikes of the transverse force is from the movement of a previously shed concentration of vorticity beneath the bottom surface of the cylinder.

For the case where a finite-wavelength free-surface wave interacts with a stationary cylinder immediately beneath the free surface, Oshkai & Rockwell (1999) have shown that the orbital particle trajectory of the wave leads to multiple sites of onset of vorticity concentrations about the surface of the cylinder and thereby multiple locations of vortex shedding from the cylinder during a single wave cycle. These features can be altered substantially by varying the nominal degree of submergence of the cylinder beneath the free surface. In an earlier investigation, Miyata & Lee (1990) undertook a numerical simulation of wave–cylinder interaction and exhibited interesting patterns of vorticity, but for relatively low Keulegan–Carpenter number and for relatively large gap between the free surface and the cylinder; as a consequence, the influence of the free surface is not evident. Further, related investigations of a free-surface wave past a stationary cylinder are summarized by Oshkai & Rockwell (1999). Considerable insight has been provided on various aspects of the unsteady loading, but no explicit link has been established between quantitative patterns of vorticity about the cylinder in the presence of an adjacent free surface.

The foregoing investigations have involved either steady or oscillatory relative motion between the fluid and the cylinder, in the presence of an adjacent free surface. The relative motion for these cases is, for the most part, aligned in the horizontal direction. On the other hand, certain surface-piercing bodies can undergo vibrations in the vertical direction. An essential feature is generation of ordered patterns of vorticity, which, in certain cases, is associated with distortion of the free surface,

as shown by Ananthakrishnan (1997) and Ananthakrishnan & Young (1992). More explicitly, they consider heaving (vertical) oscillations of a rectangular cylinder in quiescent fluid.

All of the aforementioned investigations have provided considerable insight and serve as a basis for the present study of in-line (horizontal) oscillations of a cylinder close to a free surface in the presence of a steady current. To date, this aspect of flow–structure interaction has remained relatively unexplored, and therefore a number of important issues are unresolved. The possible occurrence of locked-on states of vortex formation is an intriguing prospect; they may exhibit analogies to the well-known lock-on due to transverse oscillations of a cylinder in the absence of a free surface. If such locked-on states are attainable, it would be important to characterize the degree to which a finite current and a defined gap between the cylinder and the free surface either stabilize or destabilize the occurrence of lock-on. Moreover, unlike the case of a cylinder undergoing in-line oscillations in quiescent fluid, a steady current past the oscillating cylinder immediately adjacent to a free surface may give rise to large-scale zones of flow separation upstream of the cylinder. Such separated zones could lead to generation of organized concentrations, which could impinge upon the cylinder. These patterns of incident vorticity are, in turn, expected to influence the formation of concentrations of vorticity in the near wake of the cylinder. The unsteady nature of these vortex systems would dictate the time variation of the in-line and transverse forces. A proper understanding of these phenomena requires their characterization in terms of instantaneous patterns of vorticity and streamline topology. The present study employs a technique of high-image-density particle image velocimetry and simultaneous force measurements to address these issues.

## 2. Experimental system and techniques

A specially designed, large-scale water channel, which allowed quantitative imaging, was employed for this investigation. Details are provided in the companion manuscript of Cetiner & Rockwell (2001), as well as by Cetiner (1998). The main test section of the channel has the following dimensions: depth of 610 mm, width of 914 mm, and length of 4928 mm. For each experiment, depending upon the desired degree of submergence of the cylinder beneath the free surface, the water depth was adjusted to one of two levels: 352 mm and 543 mm. To ensure a well-defined inflow, the main test section is preceded by a 2 : 1 contraction housing arrangements of honeycombs and screens, which provided a turbulence intensity less than 0.1%. For the present experiments, the velocity was either  $U = 35$  or  $80 \text{ mm s}^{-1}$ , which represent values of Reynolds number  $Re = 917$  and  $2075$ .

As a prelude to the present experiments, which focus on the effects of an adjacent free surface, an extensive series of experiments was performed for a fully submerged cylinder, where the free surface is sufficiently far above the cylinder such that it does not influence the wake development from, and loading of, the cylinder. This series of experiments is described by Cetiner & Rockwell (2001). Complete details of the experimental system are given by Cetiner (1998). For the present investigation, the same experimental apparatus and approaches were employed. The cylinder had a diameter of 25.4 mm and a length of 318 mm. Its orientation was horizontal, and it was mounted in a cantilevered fashion between two thin circular endplates of 368 mm diameter and 6.4 mm thickness. At one end, the cylinder was connected to a rigid arm, located exterior to the endplate, by means of a brass strain-gauge sting, which had a 6.35 mm square cross-section; a total of eight strain gauges were mounted on

the flat faces of this brass sting, in order to allow simultaneous measurement of the in-line and transverse forces. The other end of the cylinder was free and unsupported. Special care was taken to ensure that the adjacent endplate did not interfere with the measured force. At the end of the cylinder that connected to the cantilevered strain-gauge sting, a specially designed opening in the far endplate ensured that there was no contact between the endplate and the strain-gauge sting. At the opposite, free end of the cylinder, a gap of 1 mm was maintained between the interior of the endplate and the tip of the cylinder.

The location of the centre of the cylinder beneath the free surface is designated as  $h_0$ . For the reference case of the fully submerged cylinder,  $h_0 = 298$  mm. Preliminary experiments were undertaken to determine the most representative values of  $h_0$  for examining the effect of an adjacent free surface. These representative values were determined to be  $h_0 = 17.5$  mm, for which a small, but finite, gap existed between the free surface and the upper surface of the cylinder, allowing flow through the gap during a portion of the oscillation cycle; and  $h_0 = 14.3$  mm, for which the gap was sufficiently small that flow is precluded between the free surface and the surface of the cylinder. In dimensionless form, the respective values of  $h_0$  normalized with respect to the diameter  $D$  of the cylinder are  $h_0/D = 0.56, 0.69$  and  $11.73$ .

The in-line and transverse forces on the cylinder were measured by a high-sensitivity strain-gauge sting. The resonant frequency of the entire sting–cylinder system was approximately 20 Hz.; this frequency compares with the frequency of oscillation of the cylinder,  $f_e = 0.28$  Hz. Care was taken to ensure that during the cycle of oscillation of the cylinder, the endplates did not come into contact with either end of the cylinder. Details of this arrangement and calibration and verification procedures are given by Cetiner (1998) and Cetiner & Rockwell (2001). The transverse  $C_y$  force coefficient is defined as  $C_y = F_y / \frac{1}{2} \rho U_0^2 LD$ , in which  $U_0$  is the peak value of the cylinder velocity  $U_c$  at a reference Keulegan–Carpenter number  $KC = 2\pi A/D = 6.0$ . An analogous definition holds for  $C_x$ . The corresponding value in terms of the steady free-stream velocity  $U$  is  $C_y^* = F_y / \frac{1}{2} \rho U^2 LD$ , or analogously  $C_x^*$ . The value of  $U$  can be calculated from the equation  $U = f_e D / (0.2 f_e / f_0)$  in which  $f_0$  is the frequency of inherent Kármán shedding from the stationary cylinder.

Controlled motion of the cylinder in the horizontal direction was attained via a high-resolution, computer-controlled stepping motor, in turn linked to the central microcomputer system, which provided precise control of both the frequency and amplitude of the motion. The amplitude  $A$  of the cylinder oscillation was selected after preliminary experiments, which defined the minimum amplitude for the onset of pronounced antisymmetrical vortex shedding when no current  $U$  is present. This amplitude is represented by the Keulegan–Carpenter number  $KC = 2\pi A/D = 6$ , in which  $D$  is the cylinder diameter. For all experiments, the frequency  $f_e$  of oscillation of the cylinder was maintained at  $f_e = 0.28$  Hz, which corresponds to frequency parameter  $\beta = f_e D^2 / \nu = 184$ .

Variations in the dimensionless frequency  $f_e/f_0$  were attained by varying the free-stream velocity  $U$ ; the corresponding values of Reynolds number were confined to  $917 \leq Re \leq 2075$ . The values of  $f_e/f_0$  employed in this study were determined from the experiments of Cetiner & Rockwell (2001) for the fully submerged cylinder. Therein, values of  $f_e/f_0$  were varied over a wide range, allowing identification of locked-on and quasi-locked-on states of vortex formation, which occurred at values of  $f_e/f_0$  of approximately 0.5, 1.0 and 2.0. More specifically, pronounced lock-on states, associated with relatively large values of transverse force coefficient  $C_y$ , occurred at values of the frequency ratio  $f_e/f_0 = 0.44$  and 1.0 respectively. These excitation conditions are

referred to as approximately subharmonic and harmonic excitation respectively. The present investigation aims to determine the degree to which the locked-on modes of vortex formation, which correspond to these cases of excitation, were either modified or transformed entirely to new modes in the presence of an adjacent free surface.

Acquisition of instantaneous images of the velocity fields and, in turn, patterns of vorticity and corresponding streamline topology, were obtained using a laser-scanning version of high-image-density particle image velocimetry (PIV), described in detail by Rockwell *et al.* (1993). This acquisition of images was undertaken simultaneously with measurements of the instantaneous in-line and transverse forces. Laser illumination was provided by a continuous argon-ion laser with a maximum power output of 25 W. This continuous beam passed through an optical train, then impinged upon a rotating, multi- (48) faceted polygon mirror, thereby providing an effective scan rate of the laser beam of either 150 or 300 cycles  $s^{-1}$ , depending on the value of the free-stream velocity. Multiply-exposed images of 12  $\mu m$  particles were obtained using a motor-driven 35 mm camera. It had a maximum framing rate of 5.6 frames per second. This corresponds to 20 frames of the oscillation cycle of the cylinder. The particle images were recorded on 35 mm film having a high resolution of 300 lines  $mm^{-1}$ . Directional ambiguity of the particle image pattern was overcome by implementing a bias (rotating) mirror directly in front of the camera lens. By maintaining the angle of rotation of the mirror much smaller than  $1^\circ$ , systematic distortion errors were precluded.

The patterns of particle images on the 35 mm negatives were digitized at 125 pixels  $mm^{-1}$ . Employing an effective window size of 90 pixels, the digitized pattern of particle images was evaluated using a single-frame, cross-correlation technique. The window size was minimized, but maintained large enough to ensure that a minimum of approximately 50 particle images existed within the window. During the interrogation process, a 50% overlap was employed. The effective grid size on the 35 mm negative was 0.36 mm  $\times$  0.36 mm and in the plane of the laser sheet, it was 2.1 mm  $\times$  2.1 mm, dictated by the magnification  $M = 1 : 6$ . Proper experimental procedure and optimization of parameters associated with acquisition of PIV images can yield an extremely high rate of success throughout the flow field; exceptions typically occur in the region very near boundaries. In this region, invalid velocity vectors may occur due to a number of causes: (a) a vertical offset between the axis of the cylinder and the axis of the camera lens system for cases where the cylinder is displaced vertically towards the free surface; (b) an unavoidable horizontal offset between the axes of the camera lens and the cylinder during horizontal oscillations of the cylinder; (c) variable condition of the water during the course of an experiment, which influences the level of background noise and thereby the detectable images in the vicinity of the boundary of the cylinder; (d) small variations in local seeding density, which may be accentuated near the surface of the cylinder; and (e) a shadow effect on the upper side of the cylinder due to a combination of lack of perfect transmission through the window of the cylinder and partial reflection of laser light from the free surface back to the upper surface of the cylinder. The end consequence of all of these effects was, in the vicinity of the cylinder surface, to yield certain regions of invalid vectors at particular depths of submergence, most notably for cases near the free surface. Although interpolation through portions of these regions is a possibility, the entire affected domain was simply blanked out. These blanked out regions were defined by examining the raw PIV images and defining boundaries of regions where vectors exceeded an uncertainty threshold of 2%. This criterion was also applied to the region extremely close to the free surface.

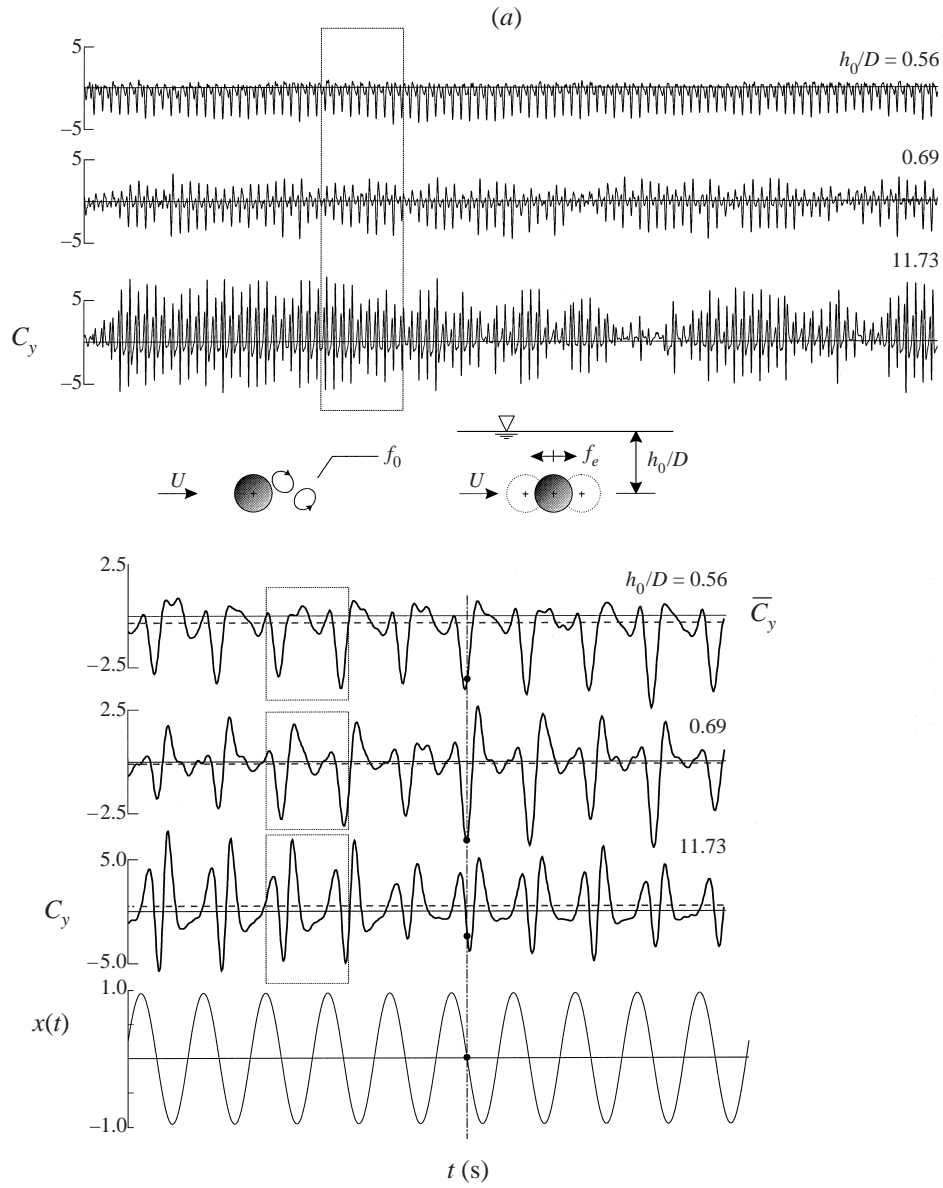


FIGURE 1(a). For caption see page 36.

### 3. Instantaneous and averaged forces

Instantaneous and time-averaged transverse and in-line forces were determined for the two principal values of frequency ratio,  $f_e/f_0$ , representing respectively subharmonic and fundamental excitation conditions, as fully described in the preceding section.

Figures 1(a) and 1(b) give time histories of the transverse force coefficient  $C_y(t)$ , for varying degrees of submergence  $h_0/D$ ; this submergence is defined in the inset of each figure. The particular values of  $h_0/D$  were determined from extensive preliminary experiments. The largest value of  $h_0/D = 11.73$  corresponds to the well-submerged

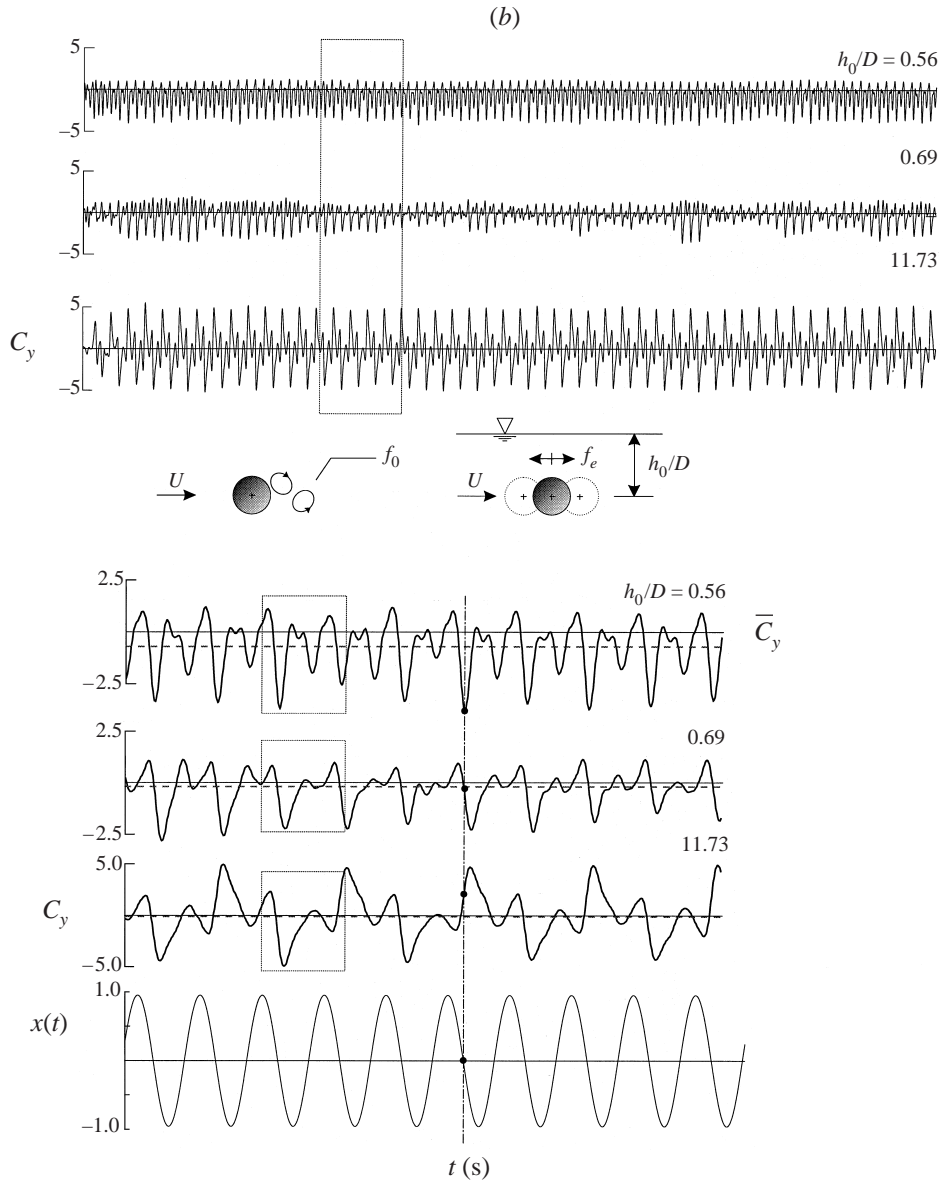


FIGURE 1. Signatures of transverse force coefficient  $C_y$  as a function of degree of submergence  $h_0/D$  beneath the free surface for controlled excitation of the cylinder at (a) approximately the subharmonic of the inherent Kármán frequency,  $f_e/f_0 = 0.44$ , and (b) the fundamental of the inherent Kármán frequency,  $f_e/f_0 = 1.00$ . Upper set of traces corresponds to long time record and lower set are expanded versions; they correspond to the section defined by the rectangular box in the upper set of traces.

cylinder, for which the presence of the free surface plays an insignificant role; this limiting case is addressed in detail by Cetiner & Rockwell (2001). At the other extreme, the smallest value  $h_0/D = 0.56$  represents the closest location to the free surface for which no flow occurs through the gap between the free surface and the upper surface of the cylinder, and for which distortions of the free surface are minimal. In between these two extremes,  $h_0/D = 0.69$  corresponds to a situation where flow occurs through



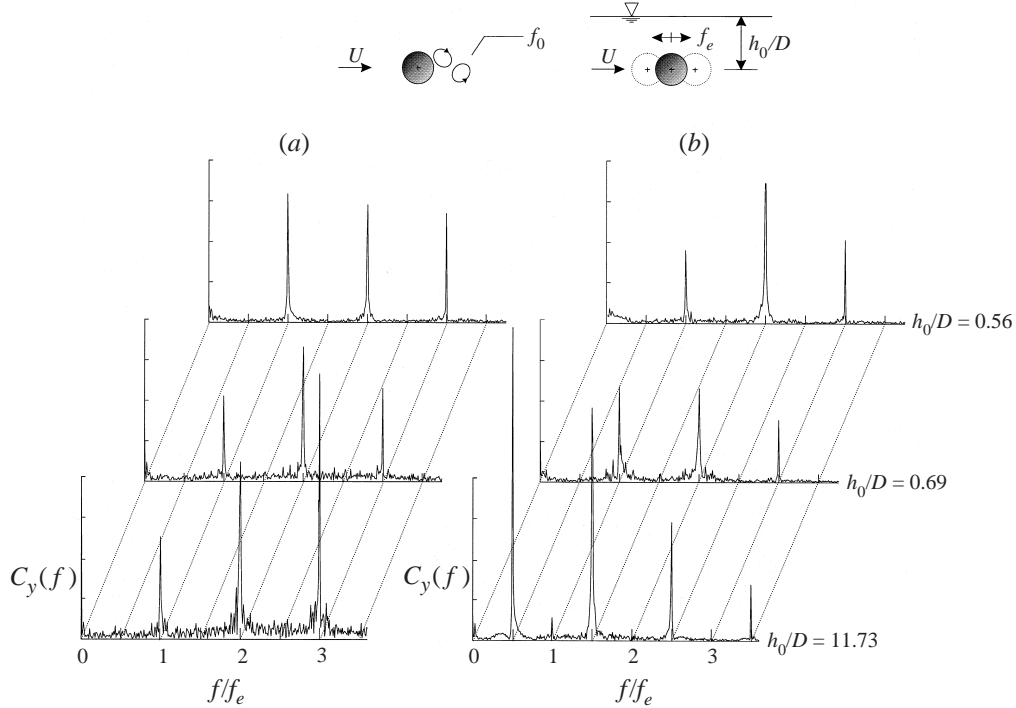


FIGURE 2. Spectra of signatures of transverse force coefficient  $C_y$ : (a) corresponds to figure 1(a) and (b) to figure 1(b).

the gap region during a portion of the oscillation cycle of the cylinder. The force coefficients in figures 1(a) and 1(b), designated as  $C_y(t)$  and  $C_x(t)$  are normalized by  $\frac{1}{2}\rho U_0^2 LD$ , as defined in the previous section.

The upper sets of traces in figures 1(a) and 1(b) correspond to long-time records of 102 cycles of the cylinder motion. It is evident that all of these force traces exhibit segments of repeatable signatures of  $C_y(t)$ . At relatively large submergence,  $h_0/D = 11.73$ , the pattern of the  $C_y(t)$  trace exhibits a relatively large amplitude and, especially in figure 1(b), a persistent pattern. In figure 1(a), corresponding to the case of subharmonic excitation, the trace repeats every cycle of the cylinder motion, whereas in figure 1(b), representing cylinder oscillation at the fundamental of the Kármán frequency, the trace repeats every second cycle. When the distance between the free surface and the cylinder is decreased to  $h_0/D = 0.69$ , corresponding to a significant gap between the free surface and the surface of the cylinder, the  $C_y(t)$  traces are generally less repetitive. In other words, the pattern of the  $C_y(t)$  fluctuation is generally destabilized relative to that of the well-submerged case, represented by  $h_0/D = 11.73$ . Finally, when the cylinder is very close to the free surface at  $h_0/D = 0.56$ , the signatures show consistent patterns of large negative spikes and small positive peaks. The repeatability of the  $C_y(t)$  signatures has again stabilized to a highly repeatable and persistent form.

The traces shown at the bottom of figures 1(a) and 1(b) are expanded portions of segments designated by the rectangular box in each set of long records. At the largest submergence  $h_0/D$ , the magnitudes of the positive peaks are large, as already suggested in the long-time traces. In fact, in figure 1(a), the peak-to-peak magnitude at  $h_0/D = 11.73$  is typically a factor of 2 larger than that at  $h_0/D = 0.56$ . (Note the

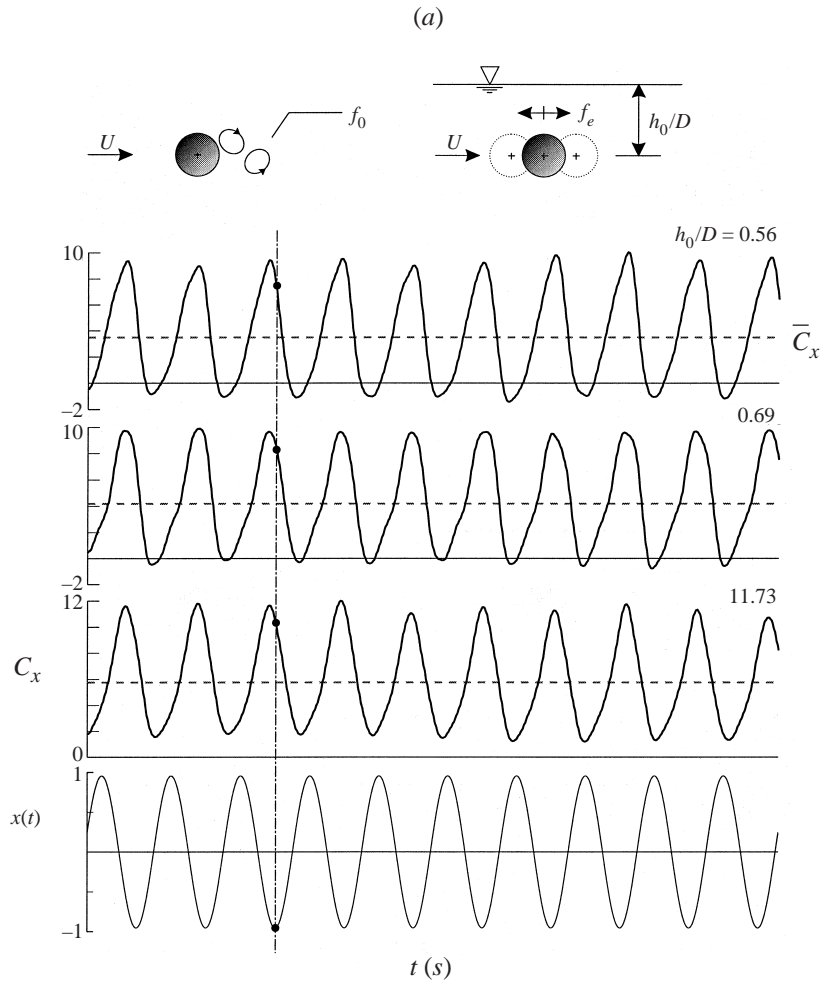


FIGURE 3(a). For caption see facing page.

difference in scale of the  $C_y$ -axis.) Moreover, for the case shown in figure 1(a), the signatures of  $C_y$  are repetitive at the same period as the cylinder displacement  $x_c(t)$  for all values of  $h_0/D$ . On the other hand, for the signatures of  $C_y$  shown in figure 1(b), the trace for the well-submerged case at  $h_0/D = 11.73$  repeats at twice the period of  $x_c(t)$ . The effect of the free-surface proximity at  $h_0/D = 0.56$  and  $0.69$  is seen to induce repetition of  $C_y(t)$  at the same period as  $x_c(t)$ .

Spectra corresponding to these signatures of  $C_y$  are given in figure 2. In all cases, at least three well-defined peaks are evident. At  $f_e/f_0 = 0.44$ , the predominant peak occurs at the third harmonic of the excitation frequency  $f_e$ , i.e.  $f/f_e = 3$ , for the case of the well-submerged cylinder ( $h_0/D = 11.73$ ). As the free surface is approached, the predominant peak shifts to lower frequencies, and at  $h_0/D = 0.56$ , it occurs at the excitation frequency  $f = f_e$ . For the case  $f_e/f_0 = 1.0$ , shown in figure 2(b), the opposite trend occurs. For the fully submerged case, the predominant peak occurs at the subharmonic of the excitation frequency  $f_e$ , i.e.  $f/f_e = 0.5$ , and when the cylinder is close to the free surface at  $h_0/D = 0.56$ , it shifts to twice the excitation frequency  $f/f_e = 2$ . Obviously, these forms of the spectra and the corresponding time signatures

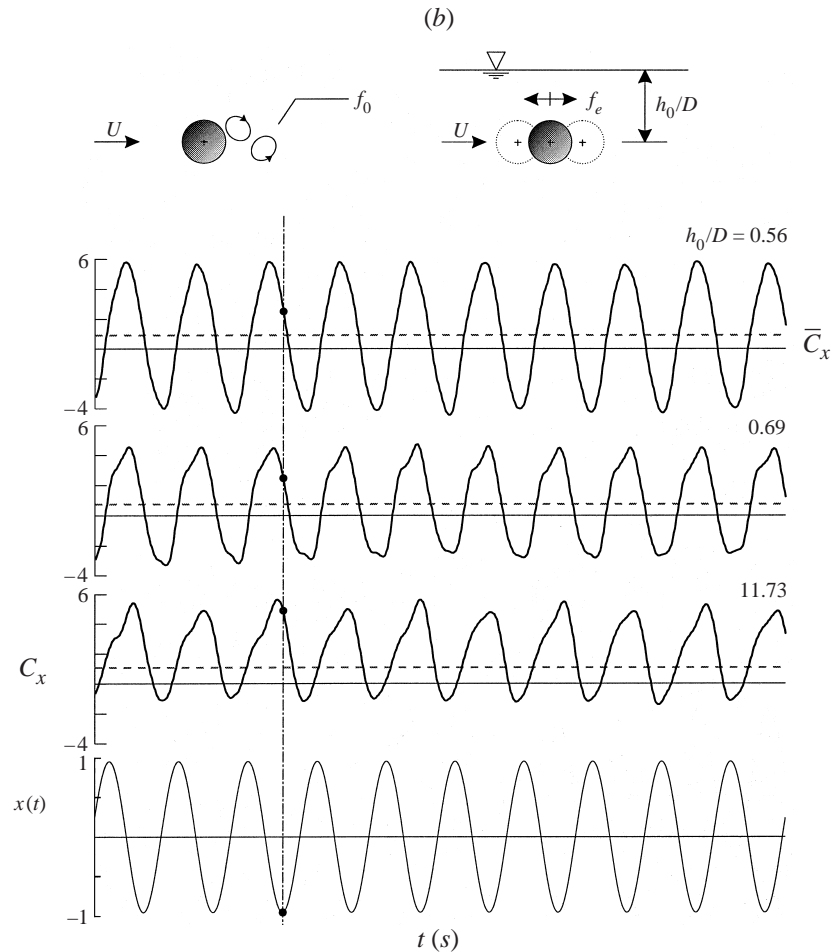


FIGURE 3. Signatures of in-line force coefficient  $C_x$  as a function of the degree of submergence  $h_0/D$  beneath the free surface. Controlled oscillation of cylinder is (a) at approximately the subharmonic of the inherent Kármán frequency,  $f_e/f_0 = 0.44$ , (b) at the fundamental of the inherent Kármán frequency,  $f_e/f_0 = 1.00$ .

of  $C_y$  are intimately related to the flow structure of the near wake, to be addressed subsequently.

Time-dependent variations of the in-line force coefficient  $C_x$  are indicated in figures 3(a) and 3(b) for approximate subharmonic and fundamental excitation frequency ratios  $f_e/f_0 = 0.44$  and 1.0. It is evident that these fluctuations occur at a predominant frequency equal to the oscillation frequency of the cylinder. Variations in the level of submergence  $h_0/D$  are seen to produce little change in peak-to-peak amplitude in figure 3(a). On the other hand, for excitation at the fundamental, shown in figure 3(b), when the cylinder is moved to a location immediately beneath the free surface, the peak-to-peak amplitude exceeds that of the well-submerged cylinder by about 40%. In both figures 3(a) and 3(b), however, there is little change in the phase shift of the  $C_x(t)$  trace relative to the cylinder displacement  $x_c(t)$ ; the black dots on each of the traces serve as a phase reference.

The time-averaged values of the transverse force  $\bar{C}_y$  are substantially influenced by the presence of the free surface. A horizontal dashed line representing  $\bar{C}_y$  is shown on

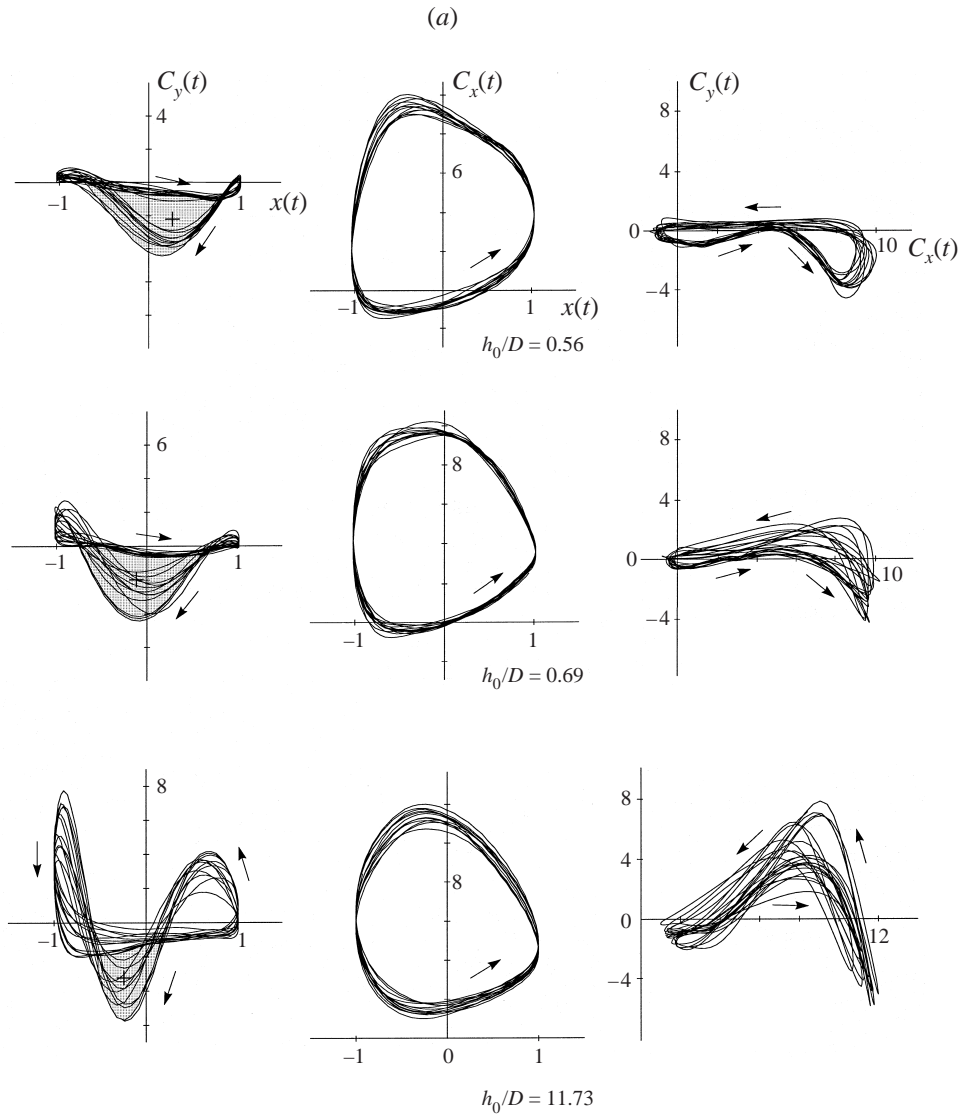


FIGURE 4(a). For caption see facing page.

the expanded signatures in figures 1(a) and 1(b). These averaged values were obtained from the longer records shown at the top of each figure. As already pointed out in §2, the definition of  $C_y$  is based on the maximum amplitude of the unsteady velocity of the cylinder. In order to obtain a value of force coefficient  $C_y^*$  based on the steady inflow velocity, it is necessary to multiply  $C_y$  by 0.282 for figure 1(a) corresponding to  $f_e/f_0 = 0.44$  and by 1.446 for figure 1(b) corresponding to  $f_e/f_0 = 1.0$ . Particularly remarkable are the relatively large magnitudes of negative  $\bar{C}_y = -0.67$  and  $-0.70$  shown respectively in figures 1(a) and 1(b) for the case of the cylinder immediately beneath the free surface ( $h_0/D = 0.56$ ). This onset of a substantial value of  $\bar{C}_y$  in the downward direction is related to the pronounced negative spikes in the time trace  $C_y(t)$ . The existence of a finite gap ( $h_0/D = 0.69$ ) yields significantly smaller values of  $\bar{C}_y = -0.20$  in both figures 1(a) and 1(b). Note the positive value of the

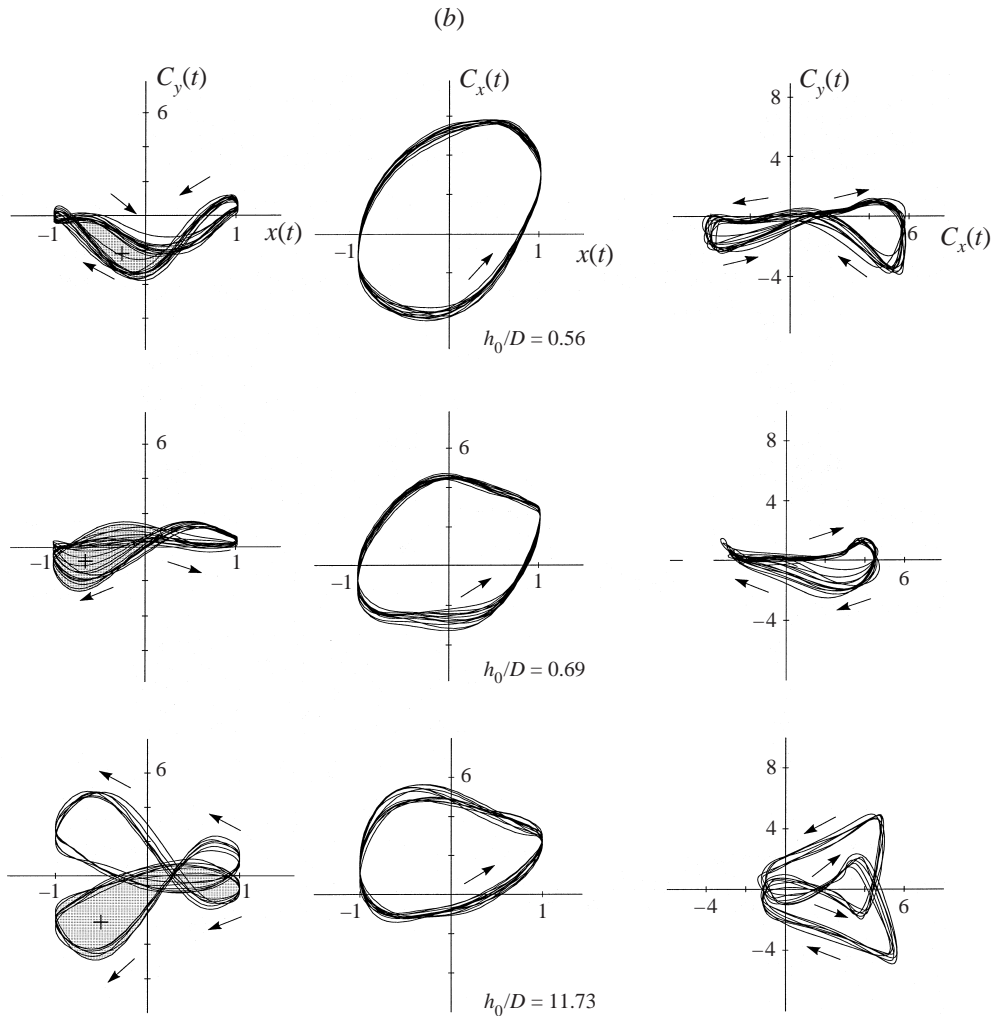


FIGURE 4. Lissajous patterns of force coefficients for oscillation of cylinder at (a) approximately the subharmonic of the Kármán frequency,  $f_e/f_0 = 0.44$ , and (b) the fundamental of the Kármán frequency,  $f_e/f_0 = 1.00$ .

averaged transverse force coefficient at the largest submergence  $h_0/D = 11.73$  in figure 1(a). This is apparently due to an asymmetry in the vortex formation process from the cylinder; finite values of transverse force coefficient have been documented for oscillatory flow past a stationary cylinder due to asymmetry of the vortex shedding process by Obasaju, Bearman, and Graham (1988).

The averaged value of the in-line force coefficient  $\bar{C}_x$  is also substantially altered relative to that for the case of the fully submerged cylinder, as shown in figures 3(a) and 3(b). For both cases, when the cylinder is adjacent to the free surface, the magnitude of  $\bar{C}_x$  decreases relative to its fully submerged value. In figure 3(a),  $\bar{C}_x = 3.49, 4.19$  and  $5.78$  respectively for  $h_0/D = 0.56, 0.69$  and  $11.73$ . In figure 3(b),  $\bar{C}_x = 0.91, 0.76$  and  $1.08$  for  $h_0/D = 0.56, 0.69$  and  $11.73$ .

Further representations of the force coefficients  $C_y(t)$  and  $C_x(t)$  are given in figures 4(a) and 4(b), which provide several types of Lissajous patterns. These plots were

obtained by considering 12.5 cycles of the cylinder oscillation. Considering first the plots of figure 4(a), the effect of proximity to the free surface ( $h_0/D = 0.56$  and  $0.69$ ) is to produce positive (clockwise) hysteresis loops lying largely in the lower half-plane of the  $C_y$  vs.  $x_c$  plots. At the deepest submergence,  $h_0/D = 11.73$ , negative hysteresis loops of substantial extent occur in the upper half-plane. Regarding the trajectories of  $C_x(t)$  vs.  $x_c(t)$ , these loops have a generally similar form irrespective of the level of submergence. Finally, the trajectories of  $C_y(t)$  vs.  $C_x(t)$  shown in the right-hand column of figure 4(a) are essentially confined to the lower half-plane when the cylinder is located immediately beneath the free surface ( $h_0/D = 0.56$ ). At larger values of submergence ( $h_0/D = 0.69$  and  $11.73$ ), the trajectories of  $C_y(t)$  vs.  $C_x(t)$  are less congruent for successive cycles; moreover, they occur largely in the upper half-plane.

The plots of figure 4(b) again show, for the case of the cylinder oscillation immediately adjacent to the free surface ( $h_0/D = 0.56$ ), that the signatures  $C_y(t)$  vs.  $x_c(t)$  and  $C_y(t)$  vs.  $C_x(t)$  are essentially confined to the lower half-plane. This observation again emphasizes the inhibiting influence of the free surface. When the cylinder is located further beneath the free surface, such that a gap exists ( $h_0/D = 0.69$ ), a larger fraction of the hysteresis loop lies in the upper half-plane; moreover, the trajectories are less congruent from cycle to cycle of the cylinder oscillation, again indicating increased phase variations between the loading and the cylinder motion. At the deepest submergence  $h_0/D = 11.73$ , remarkable congruent and symmetrical shapes of both  $C_y(t)$  vs.  $x_c(t)$  and  $C_y(t)$  vs.  $C_x(t)$  are attained in the upper and lower half-planes.

Taking an overview of figures 4(a) and 4(b), it is evident that the highly repetitive, essentially congruent trajectories shown in the top rows corresponding to the cylinder immediately beneath the free surface ( $h_0/D = 0.56$ ), indicate phase-locking between the cylinder loading and its motion, and we therefore conclude that the effect of the free surface is to stabilize the fluctuations of the loading relative to the cylinder displacement. On the other hand, the Lissajous patterns in the second row of figures 4(a) and 4(b) indicate a definite decrease in repeatability, due to loss of phase-locking. As will be shown subsequently, this tendency towards destabilization is due to a jet-like flow between the free surface and the surface of the cylinder; in contrast, such a jet flow is precluded when the cylinder is immediately beneath the free surface. Finally, when the cylinder is well-submerged, corresponding to the bottom row of Lissajous patterns in figures 4(a) and 4(b), highly phase-locked trajectories are attainable at the fundamental excitation frequency shown in figure 4(b); well-defined trajectories, but with less phase-locking, which correspond to a quasi-locked-on state, are evident at the subharmonic excitation in figure 4(a).

The Lissajous trajectories of the in-line force coefficient  $C_x(t)$  versus streamwise displacement  $x_c(t)$  described in the foregoing are directly related to the energy transfer between the cylinder and the fluid. Blackburn & Henderson (1999) computed the energy transfer associated with the transverse force on a cylinder undergoing oscillations in the cross-stream direction. By analogy, the area enclosed by the in-line force  $C_x(t)$  versus in-line displacement  $x_c(t)$  trajectories of figures 4(a) and 4(b) represents the energy transfer between the fluid and the cylinder. Since the direction of these trajectories is counterclockwise, the energy transfer is from the cylinder to the fluid. In figure 4(b), for example, the area enclosed by the Lissajous trajectory, and thereby the energy transfer, is larger when the cylinder is immediately beneath the free surface ( $h_0/D = 0.56$ ) than when it is well submerged ( $h_0/D = 11.73$ ).

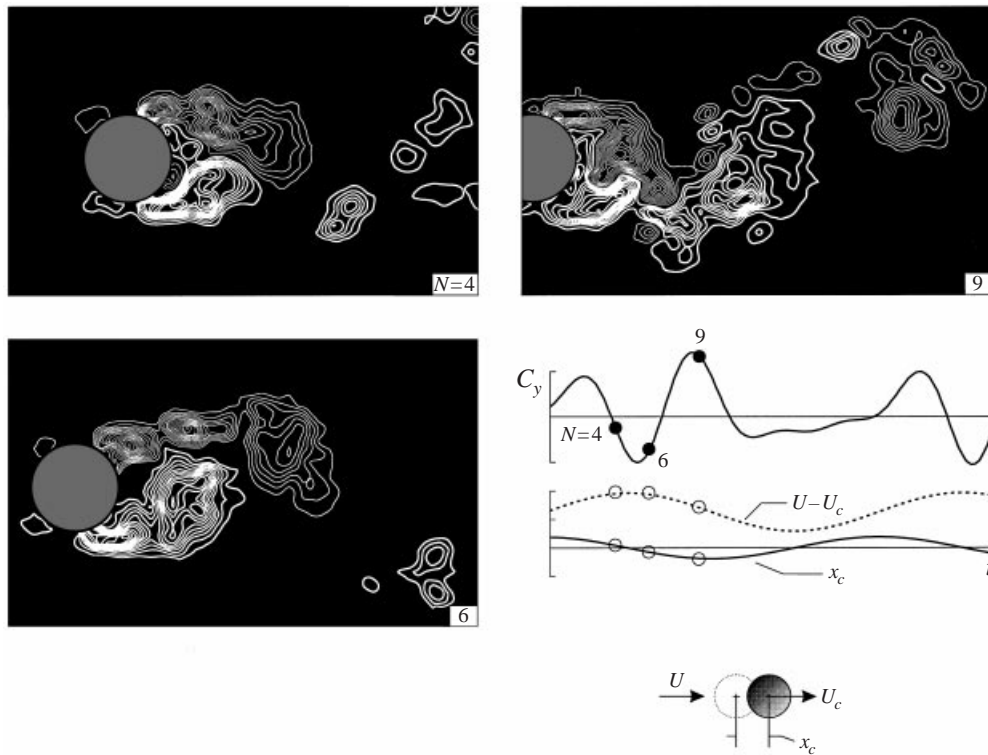


FIGURE 5. Patterns of vorticity and corresponding signature of transverse force coefficient  $C_y$  for the case of a well-submerged cylinder at a depth  $h_0/D = 11.73$ . Cylinder excitation frequency is  $f_e/f_0 = 0.44$ .

#### 4. Patterns of vorticity

##### 4.1. Vorticity patterns due to oscillation at the subharmonic of Kármán frequency

*Well-submerged cylinder.* For the case of the well-submerged cylinder ( $h_0/D = 11.73$ ) oscillating at approximately the subharmonic frequency,  $f_e/f_0 = 0.44$ , the patterns of vorticity and the corresponding transverse force coefficient  $C_y$  take the forms shown in figure 5; they are taken from Cetiner & Rockwell (2001). The symbol  $N$  represents the frame number of the cinema PIV sequence. The relation between  $N$  and the instantaneous position and relative velocity of the cylinder are given in the inset of figure 5. When the fully formed negative (grey–clockwise) vortex moves away from the cylinder, evident in images  $N = 4$  and 6, a negative peak occurs on the  $C_y(t)$  trace. On the other hand, the positive (white–counterclockwise) vortex, which continues to develop near the base region in images  $N = 4$  and 6, in turn moves away from the cylinder, contributing to a positive peak at  $N = 9$ .

*Cylinder beneath the free surface: consequence of a finite gap.* When the cylinder is close to the free surface but a finite gap exists ( $h_0/D = 0.69$ ), such that flow occurs between the free surface and the cylinder during part of the oscillation cycle, the vortex formation and correspondingly the transverse force are remarkably altered, as exhibited in figure 6. The principal types of vortex formation are shown in the image  $N = 2$ . Positive (white) and negative (grey) concentrations of vorticity form respectively from the lower and upper surfaces of the cylinder. Since formation of

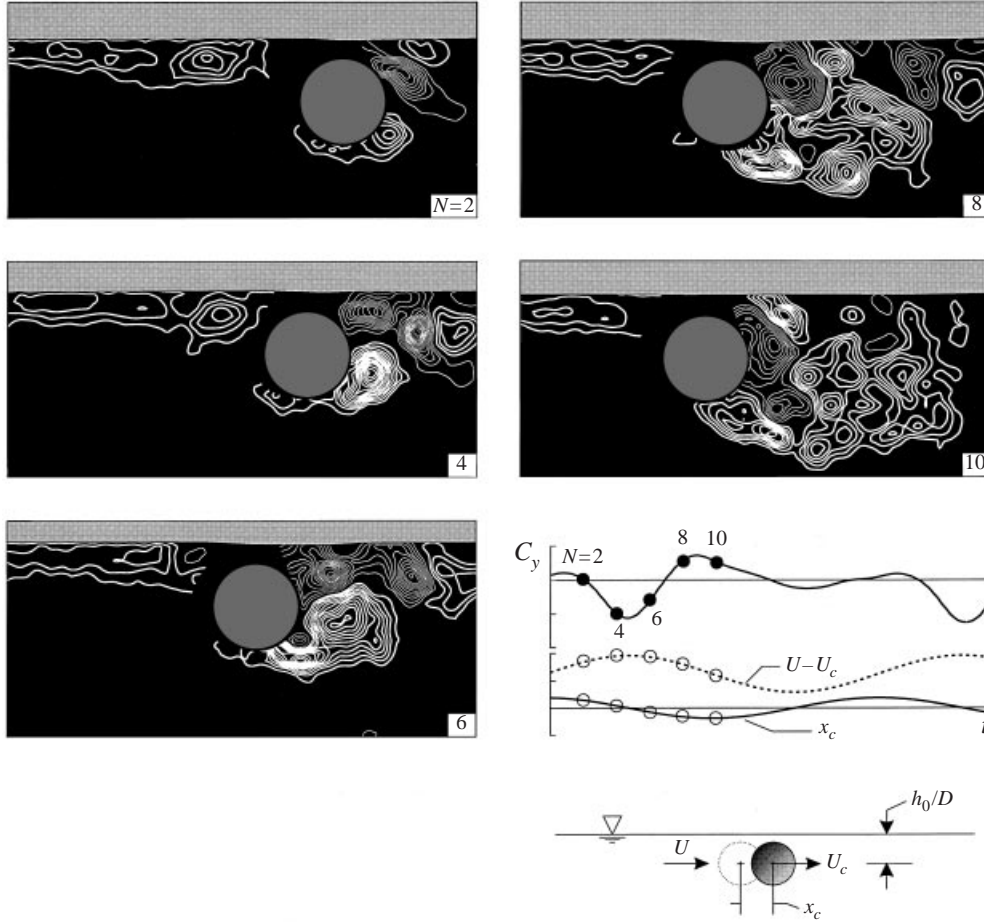


FIGURE 6. Patterns of vorticity and corresponding signature of transverse force coefficient  $C_y$ . Depth of submergence is  $h_0/D = 0.69$ ; dimensionless frequency of oscillation of cylinder is  $f_c/f_0 = 0.44$ .

the negative concentration occurs adjacent to the free surface, it induces formation of a small-scale positive concentration, and together they form a counter-rotating vortex pair. Upstream of the cylinder, a positive vorticity layer, arising from the tangential velocity gradient along the free surface imposed by presence of the cylinder, agglomerates to form a concentration of positive vorticity. Vorticity generation at a free surface has been described by Rood (1990, 1995), Gharib & Weigand (1996) and Dabiri & Gharib (1997). For a constant-pressure free surface, the vorticity flux is

$$v \left( \frac{\partial \omega}{\partial n} \right)_{n=0} = -\frac{\partial u_s}{\partial t} - g \cos \theta - \left( \frac{1}{2} \right) \frac{\partial u_s^2}{\partial s}, \quad (1)$$

where  $n$  and  $s$  are coordinates perpendicular and tangent to the free surface,  $\omega_z$  is the vorticity component perpendicular to the  $(xy)$ -plane,  $\theta$  is the angle between  $s$  and the horizontal and  $u_s$  is the tangential velocity component, i.e. the component parallel to  $s$ . In the present configuration, the blockage of the cylinder imposes distortion of the velocity field well upstream and thereby variations of  $u_s$  along the free surface, even if it is not significantly distorted. As a consequence, vorticity flux is due primarily



to the last term on the right-hand side of equation (1). When the cylinder oscillates, depending upon the frequency and amplitude, different types of distortion of the tangential velocity  $u_s$  will be induced immediately beneath the free surface, thereby introducing time-dependent variations of vorticity flux.

Images  $N = 2$  and 4 represent the near-wake development in relation to the onset of maximum negative  $C_y$ . The negative concentration of vorticity from the upper surface of the cylinder, as well as the positive one shed from the free surface, continue to develop as they move downstream away from the cylinder. Simultaneously, the positive cluster of vorticity continues to form from the bottom surface of the cylinder, while the distance between the positive cluster of vorticity upstream of the cylinder and the cylinder surface decreases.

In images  $N = 6$  and 8, the magnitude of  $C_y$  increases to its maximum positive value. The patterns of vorticity show that the negative cluster of vorticity originally formed from the upper surface of the cylinder has been partitioned into two independent concentrations, each with an adjacent positive concentration of vorticity induced from the free surface; in other words, a street of counter-rotating vortex pairs is located along the free surface, as indicated in the image  $N = 8$ . Simultaneously, additional concentrations of positive vorticity are shed from the lower surface of the cylinder.

Finally, in image  $N = 10$ , the cluster of positive vorticity from the bottom surface of the cylinder has become very large; it is made up of a number of small-scale concentrations. The counter-rotating vortex pair adjacent to the upper surface of the cylinder, however, has, in essence, remained in place. The region of positive vorticity upstream of the cylinder has a weaker, distributed form.

It is evident that the foregoing features of the vorticity field generation and development are considerably more complex than for the case of the well-submerged cylinder shown in figure 5. A generally common feature, however, is that the increasingly positive values of  $C_y$  occurring in images  $N = 6$  to 9 in figure 5 and  $N = 6$  to 8 in figure 6 occur in accord with movement of the large-scale concentration of positive vorticity away from the cylinder.

*Cylinder immediately beneath free surface.* When the cylinder is located immediately beneath the free surface ( $h_0/D = 0.56$ ), as shown in figure 7, study of an extensive series of images over a complete cycle of the cylinder oscillation shows that, in essence, no flow occurs in the small gap between the free surface and the upper surface of the cylinder. Nevertheless, as indicated in image  $N = 2$ , a negative (grey) cluster of vorticity forms from the upper region of the cylinder base. In addition, a positive concentration forms from the bottom surface of the cylinder, while the distributed layer of vorticity upstream of the cylinder culminates in a concentration adjacent to the cylinder surface. The onset of the maximum-negative value of  $C_y$  is accompanied by continued development of the negative and positive concentrations formed from the cylinder and, unlike the scenario exhibited in figure 6, involves downward deflection of the vorticity layer formed upstream of the cylinder; it is deflected in the downward direction away from the free surface such that its vorticity merges with that shed from the bottom surface of the cylinder.

Increasingly positive values of  $C_y$  are associated with the patterns of vorticity shown in images  $N = 4, 6$  and 8. In image  $N = 6$ , an additional negative concentration is formed from the upper region of the cylinder base, and it induces a corresponding positive concentration from the free surface. The large-scale concentration from the bottom surface of the cylinder continues to develop and move downstream. Further evolution of this type is shown in the image  $N = 8$ .

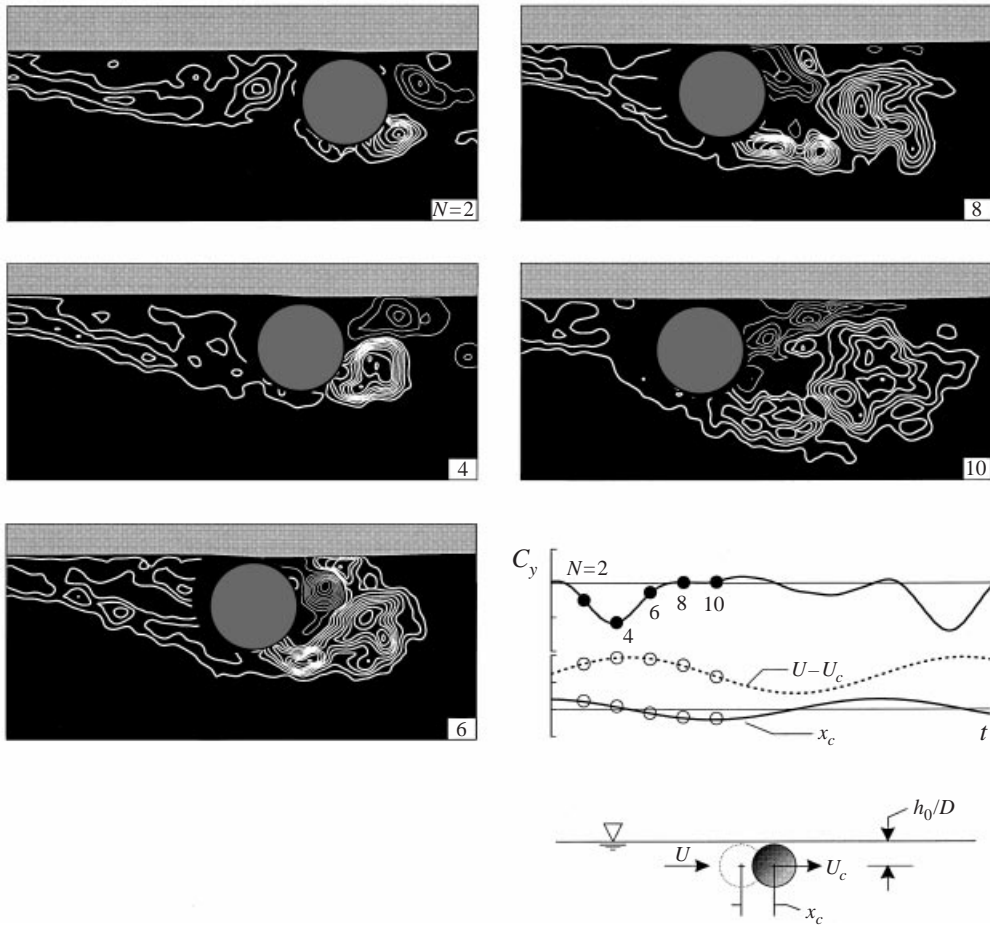


FIGURE 7. Patterns of vorticity and corresponding signature of transverse force coefficient  $C_y$ . Depth of submergence is  $h_0/D = 0.56$ ; dimensionless frequency of oscillation of cylinder is  $f_e/f_0 = 0.44$ .

Finally, in image  $N = 10$ , the large-scale cluster of positive vorticity originally formed from the bottom surface of the cylinder has induced a region of negative vorticity between it and the free surface. This, as well as other features of the vorticity patterns shown in images  $N = 6, 8$  and  $10$ , are associated with the absence of a significant positive peak in the corresponding trace of  $C_y$  in figure 7. This observation contrasts with the pronounced positive peak that occurs for the fully submerged cylinder, exhibited in figure 5, for which the patterns of vorticity evolve in the absence of free-surface effects. A common feature of the events shown in figures 5 and 7 is the increasingly positive  $C_y$  that occurs for  $N = 4$  and  $8$  in figure 7 and  $N = 6$  to  $9$  in figure 5; these changes correspond to movement of the large-scale concentration of vorticity originating from the bottom surface of the cylinder, in the downstream direction.

#### 4.2. Vorticity patterns due to oscillation at the fundamental of Kármán frequency

*Well-submerged cylinder.* For the case of the fully submerged cylinder oscillating at a frequency corresponding to the Kármán shedding frequency from the corresponding stationary cylinder, the patterns of vorticity and the corresponding transverse force

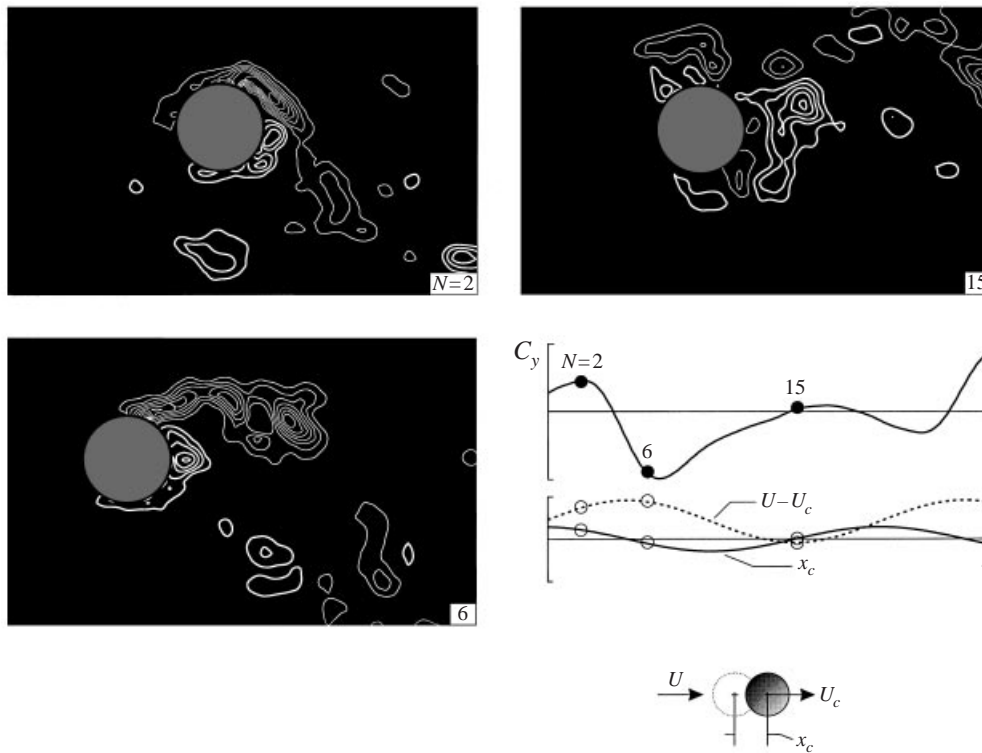


FIGURE 8. Patterns of vorticity and corresponding signature of transverse force coefficient  $C_y$  for the case of a well-submerged cylinder at a depth of submergence  $h_0/D = 11.73$ . Cylinder excitation frequency is  $f_e/f_0 = 1.00$ .

coefficient  $C_y$  take the form shown in figure 8; these images are taken from Cetiner & Rockwell (2001). Comparing images  $N = 2$  and 6, movement of the large-scale cluster of negative (grey) vorticity away from the upper surface of the cylinder contributes to the negative peak of  $C_y$  at  $N = 6$ . At a later instant, represented by  $N = 15$ , the large-scale cluster of positive (white) vorticity originally formed at  $N = 6$  from the lower surface of the cylinder is further displaced away from the cylinder. In addition, due to the rightward motion of the cylinder, a large-scale cluster of negative vorticity shed at an earlier time during the oscillation cycle now appears above the surface of the cylinder. These events contribute to increasingly positive  $C_y$  between  $N = 6$  and 15.

*Cylinder beneath the free surface: consequence of a finite gap.* The effects of proximity of the free surface, with a finite gap between the surface of the cylinder and the free surface, are represented by figure 9. In image  $N = 3$ , positive and negative vorticity concentrations form in the immediate near wake; in addition, a cluster of negative vorticity, shed from a previous cycle, appears below the cylinder. In image  $N = 7$ , the positive and negative clusters of vorticity formed from the bottom and top surfaces have further developed; each of these clusters contains two smaller-scale concentrations. Simultaneously, the negative cluster of vorticity has induced shedding of positive vorticity from the free surface; the consequence is a counter-rotating vortex pair immediately beneath the free surface. This development of the near wake, in

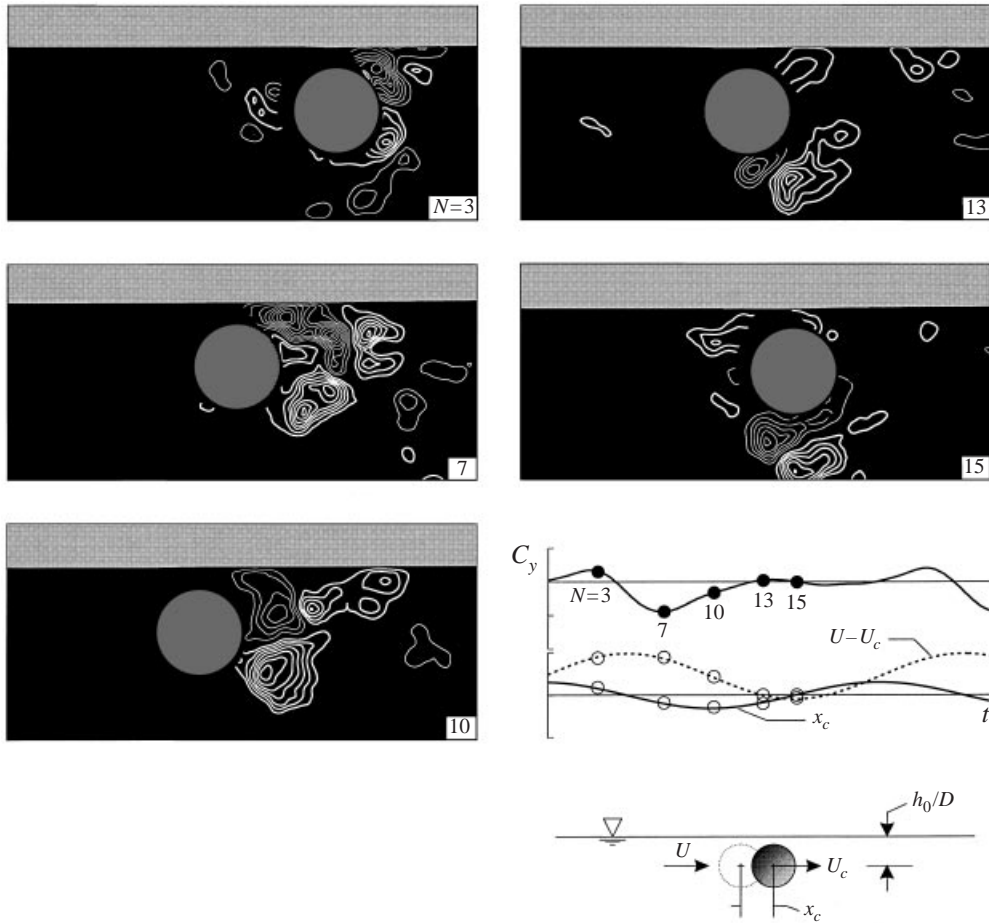


FIGURE 9. Patterns of vorticity and corresponding signature of transverse force coefficient  $C_y$ . Depth of submergence is  $h_0/D = 0.69$ ; dimensionless frequency of oscillation of cylinder is  $f_e/f_0 = 1.00$ .

going from image  $N = 3$  to 7 is associated with onset of the maximum-negative value of  $C_y$ , shown in the trace in the inset.

Image  $N = 10$  shows further development of this pattern of vorticity; shedding from the cylinder surface and the free surface are complete. At still later instants, shown in images  $N = 13$  and 15, rightward movement of the cylinder enhances shedding of new vorticity concentrations. Particularly evident in image  $N = 15$  are a positive vorticity layer from the upper surface of the cylinder and a negative layer from the bottom surface. Moreover, the previously shed positive concentration of vorticity forms a counter-rotating vortex system with the newly shed negative concentration as they both move about the bottom of the cylinder. All of these events are associated with increasingly positive values of  $C_y$ .

*Cylinder immediately beneath the free surface.* When the cylinder is located immediately beneath the free surface, represented by figure 10, the pronounced shedding of a negative layer of vorticity from the upper surface of the cylinder is inhibited, relative to that occurring in figure 9. In image  $N = 2$ , no such concentration is evident. At later times, however, represented by images  $N = 4, 8$  and 13, detectable small-

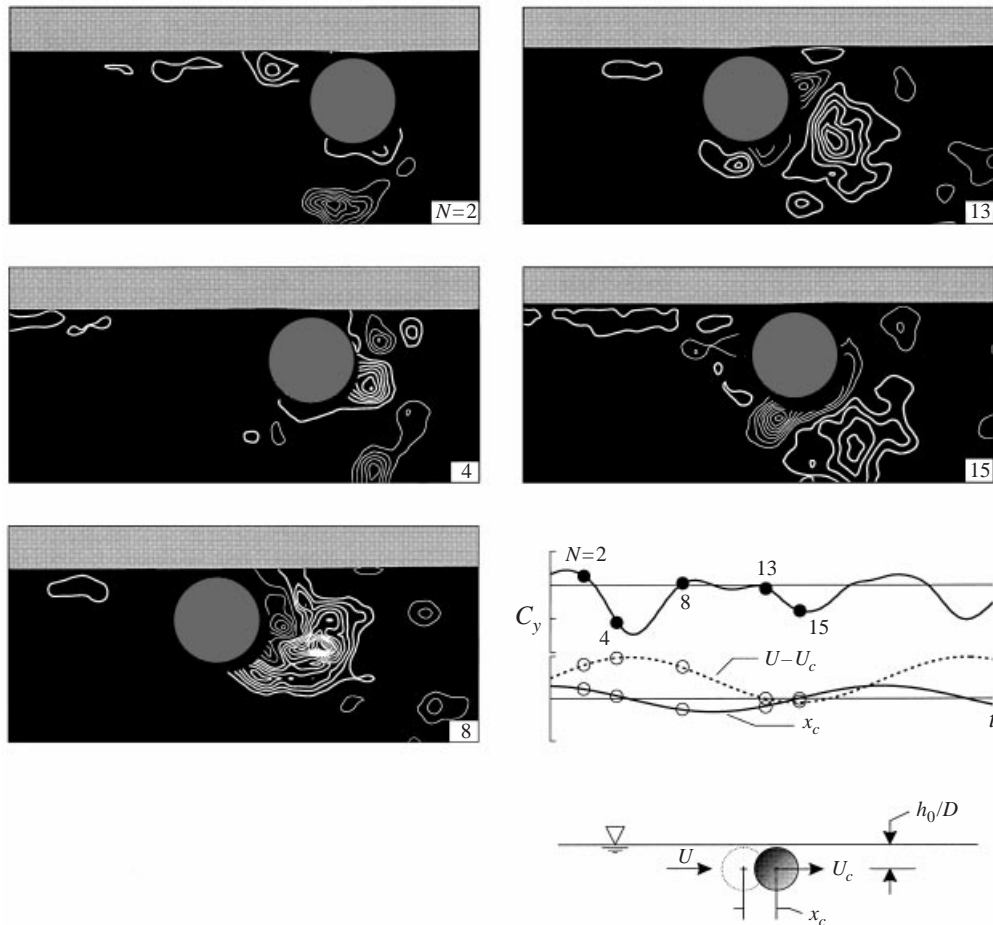


FIGURE 10. Patterns of vorticity and corresponding signature of transverse force coefficient  $C_y$ . Depth of submergence is  $h_0/D = 0.56$ ; dimensionless frequency of oscillation of cylinder is  $f_c/f_0 = 1.00$ .

scale concentrations of negative vorticity, which originate from the upper portion of the base of the cylinder, rather than from the upper shoulder of the cylinder, are discernible. Otherwise, the overall development of the patterns of vorticity of figure 10 bear general similarities to those of figure 9. The counter-rotating vortex pair formed immediately beneath the free surface at  $N = 4$  in figure 10 involves positive and negative concentrations of vorticity having substantially smaller circulation than those in the corresponding image  $N = 7$  in figure 9. Moreover, the large-scale cluster of positive vorticity formed from the bottom surface of the cylinder, clearly evident in images  $N = 8$  and 13, has a significantly larger value of circulation than that shown in  $N = 10$  of figure 9. It promotes a defined negative peak of  $C_y$  at  $N = 15$  as it passes beneath the cylinder.

All of the foregoing representations of the flow patterns involve instantaneous images. Various ensemble-averaged representations of the flow structure have been performed and will be reported in future work. In essence, for those cases where locked-on vortex formation occurs, the large-scale features of the vortex formation process are highly repetitive from cycle to cycle of the cylinder motion. In addition, the instantaneous traces of the transverse force coefficient show a highly repetitive form

for several cases; this repetition is only attainable if the large-scale structures formed from the cylinder are consistent. Of course, in those situations where substantial amplitude or frequency modulation occurs in the time-traces of the force coefficients, it is important to consider the instantaneous patterns of vorticity and velocity.

#### 4.3. Distinctions and common features of vorticity patterns

Viewing together the patterns of vorticity corresponding to the oscillation of the cylinder at the subharmonic of the Kármán frequency, shown in figures 5 to 7, and at the fundamental of the Kármán frequency given in figures 8 to 10, several distinctions appear. First of all, the formation of a large-scale region of distributed vorticity and, in some cases, vorticity concentrations, at locations upstream of the cylinder in the images of figures 6 and 7 is either indicated in weaker form, or not evident at all, in the images of figures 9 and 10. Apparently, the lower oscillation frequency of the subharmonic oscillation of figures 6 and 7 allows time for development of the large-scale separated zone immediately beneath the free surface; this lower frequency produces a pattern close to what one expects on the basis of quasi-steady or stationary cylinder considerations, i.e. formation of the large-scale separated zone upstream of the cylinder. Patterns of vorticity are detectable immediately beneath the free surface for the case where the cylinder is closest to the free surface, and excitation is at the fundamental frequency, as shown in figure 10. The level of vorticity is, however, substantially lower than that of the corresponding subharmonic excitation case of figure 7.

A further distinguishing feature is that previously shed concentrations of vorticity move upstream, i.e. beneath the surface of the cylinder, during later stages of the oscillation cycle at the fundamental frequency, as shown in figures 9 and 10. This type of event does not occur for the subharmonic excitation frequency in figures 6 and 7.

On the other hand, common features for the cases of excitation at subharmonic and fundamental frequencies involve two classes of events. First, pronounced shedding of vorticity occurs from the free surface; it is induced by the vorticity concentration originally shed from the surface of the cylinder. Formation of these counter-rotating vortex pairs is shown in figures 6, 7, and 9, 10. Second, generic to all cases is the formation of a large-scale vortex from the lower surface of the cylinder and its displacement away from the cylinder. For all scenarios, it is associated with increasingly positive values of  $C_y$ .

## 5. Topology of velocity and streamline patterns

The development of representative patterns of velocity and streamlines are exhibited in figures 11(a) and 11(b). Considering first the patterns of velocity of figure 11(a), for both values of submergence of the cylinder beneath the free surface, regions of low velocity are evident beneath the free surface at locations well upstream of the cylinder. Image  $N = 9$  in the left-hand column shows that this low-velocity domain extends all the way from the free surface to the bottom surface of the cylinder. As the cylinder moves to the right in images  $N = 15$  and 20, the vertical extent of the low-velocity region beneath the free surface (upstream of the cylinder) narrows considerably. In fact, this effect is evident in both the left- and right-hand columns of images. Moreover, swirl patterns of velocity vectors are evident immediately upstream of the cylinder in several of the images extending from  $N = 2$  to 9 in both columns of figure 11(a).

The region between the cylinder and the free surface exhibits different velocity

fields in the left- and right-hand columns of images. Images shown in the right-hand column, corresponding to the location of the cylinder immediately beneath the free surface, indicate that no net flow occurs between the cylinder and the free surface. On the other hand, images in the left-hand column, representing a finite gap between the cylinder and the free surface, clearly show a jet-like flow in the gap, especially in images  $N = 2, 9$  and  $20$ . This jet-like flow contributes to vortex formation from the upper surface of the cylinder, suggested by a swirling pattern of velocity vectors, particularly evident in images  $N = 2$  and  $9$ . It should be emphasized, however, that a jet-like flow is not essential for formation of a swirl pattern of velocity vectors near the upper surface of the cylinder. In the right-hand column, the image at  $N = 9$  shows a small-scale swirl pattern in the upper base region of the cylinder.

The corresponding streamline topology of figures 11(b) reflects the aforementioned features of the velocity fields. Formation of foci of the pattern of streamlines upstream of the cylinder, which suggests vortex formation upstream of the cylinder, is evident in both the left- and right-hand columns of images. Furthermore, formation of the large-scale vortex downstream of the cylinder, as well as initial formation of smaller vortices near the base of the cylinder, are suggested by corresponding foci. Immediately adjacent to the free surface, half- or full-saddle points are identifiable. They are designated by vertical arrows immediately above the free surface. Particularly interesting is the topology associated with formation of the large-scale vortex from the bottom surface of the cylinder. It is bounded by a limiting streamline, defined, for example, in image  $N = 9$  in the left- and right-hand columns of figure 11(b). Comparing this type of streamline pattern with the corresponding velocity field of figure 11(a) reveals that the streamline from the saddle point closest to the cylinder is tangent to downward-oriented velocity vectors, while that further downstream is associated with upward-oriented velocity vectors. This system of two saddle points near the free surface translates downstream with the large-scale vortex.

## 6. Free-surface distortions

By employing the digitized version of original PIV negatives, and considering a zoom view of a desired region of the free surface, it is possible to determine deviations from the horizontal, undisturbed state. The centroid of the interface representing the free surface could be determined within  $0.05$  mm. Although the images were originally digitized at  $125$  pixels  $\text{mm}^{-1}$ , the free-surface interface has a finite width of varying grey-level intensity, which limits the effective resolution in determining its centroid. Images corresponding to the layouts of figures 6, 7, 9, and 10 were assessed with emphasis on those images leading to onset of the maximum-negative value of  $C_y$ . A detectable local depression was centred nearly above the cylinder. For all cases, corresponding to figures 6, 7, 9, and 10, the maximum deflection of the free surface was found to be of the order of  $0.86$  mm; this deflection corresponds to  $0.034D$ , where  $D$  is the cylinder diameter.

In addition to the very small distortions of the free surface that are generated by motion of the cylinder, the degree to which concentrations of vorticity adjacent to the surface produce detectable distortions is also of interest. It is clearly evident that concentrations of both positive and negative vorticity exist close to the free surface in the images of figures 6, 7 and 9, 10. Zoomed-in analysis of the original images, using the foregoing approach, did not reveal any detectable depressions of the surface that could be linked to distinct concentrations of vorticity. For appropriate ranges of parameters, however, vortex-induced distortions are well documented in the

(a)

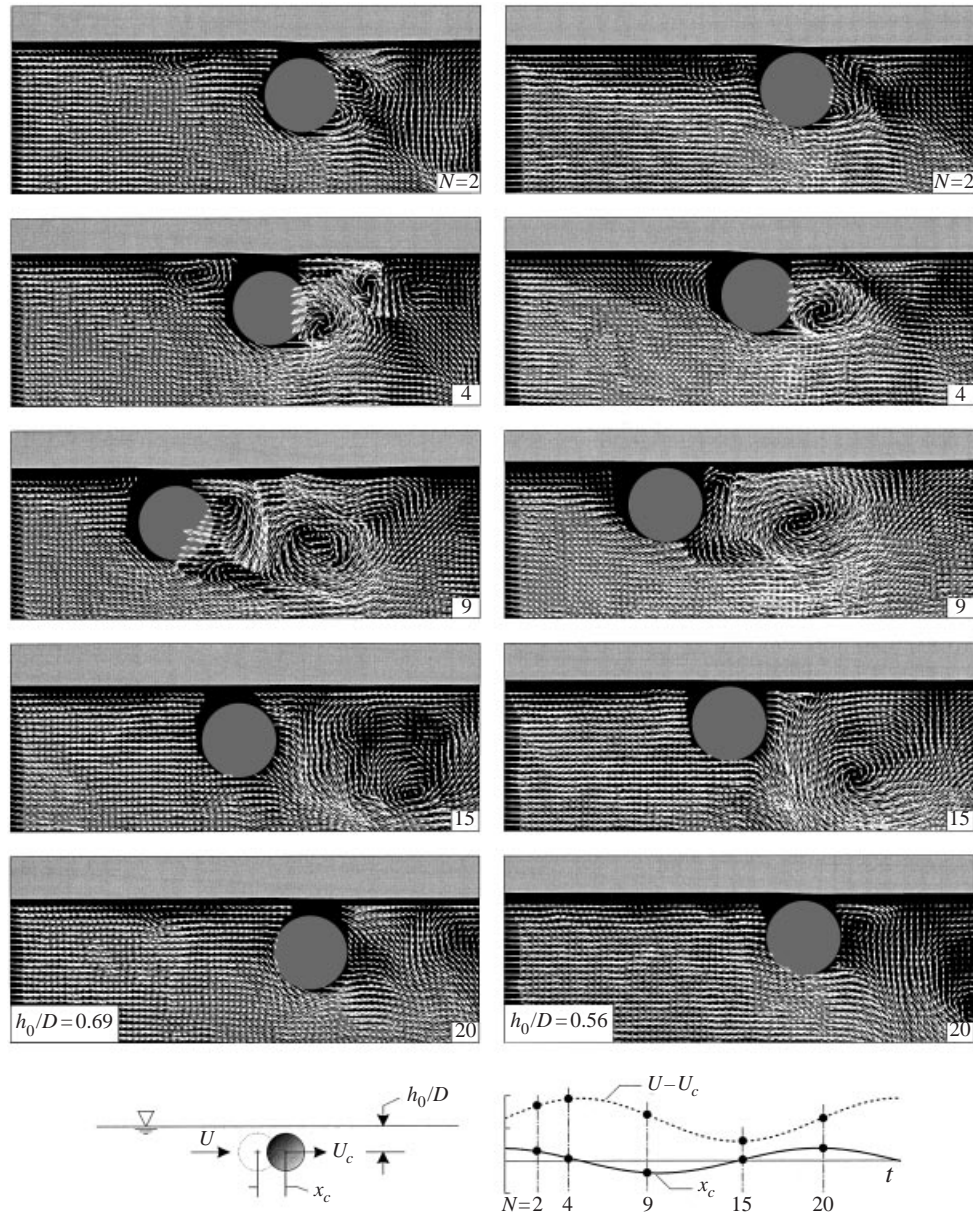


FIGURE 11(a). For caption see page 53.

numerical simulations of, for example, Lugt & Ohring (1992), Ohring & Lugt (1991), Yu & Trygavasson (1990), Sarpkaya, Magee & Merrill (1994), and Dommermuth (1993), as well as in the representative works cited therein. In essence, the principal parameters that dictate the localized vortex-induced distortion are the Froude, Weber and Reynolds numbers. Clearly, the present vortex systems involve a number of vortices, and the free-surface distortion will be a consequence of the mutual induction



(b)

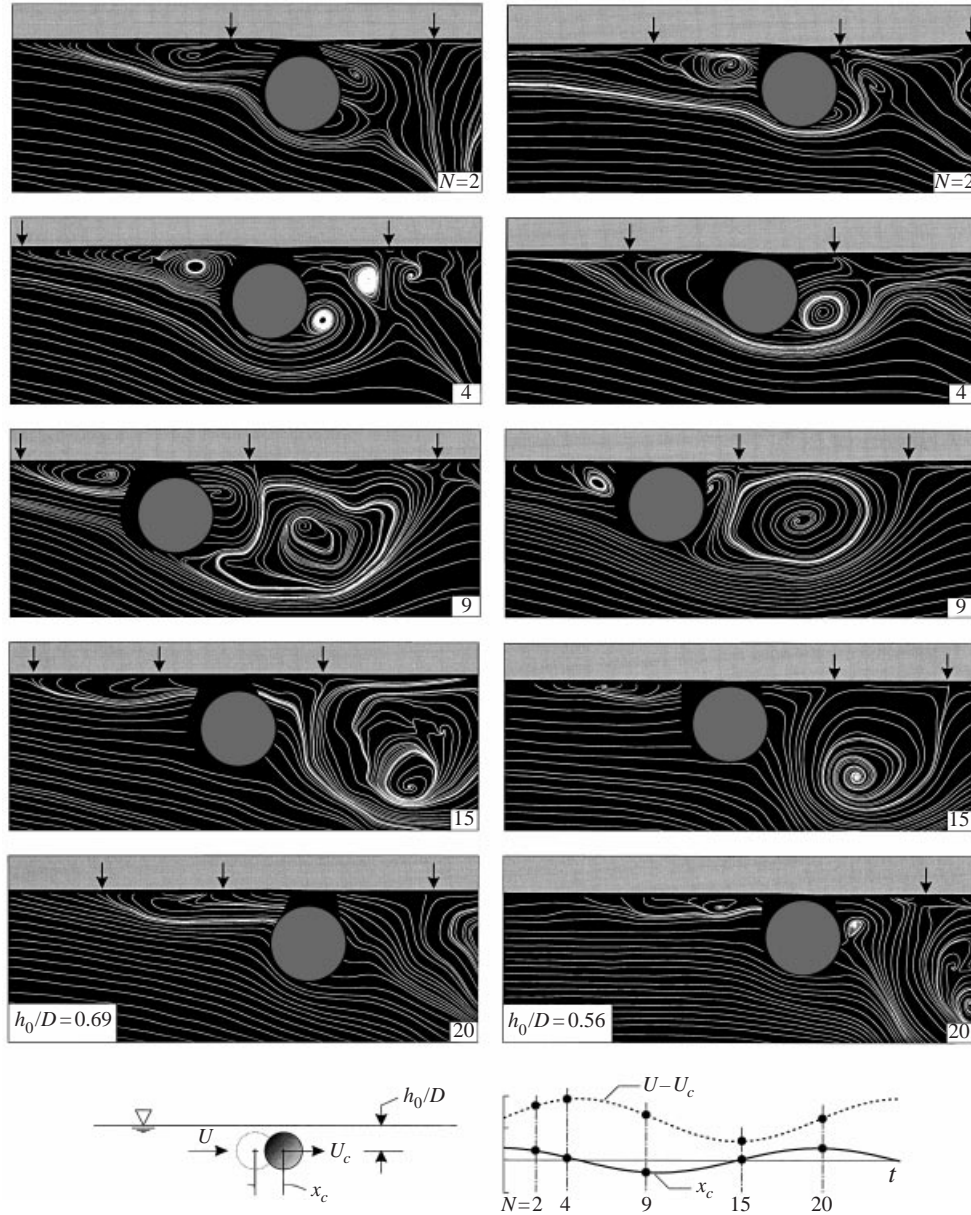


FIGURE 11. Patterns of (a) instantaneous velocity and (b) instantaneous streamlines for two levels of submergence  $h_0/D = 0.56$  and  $0.69$  in relation to instantaneous displacement  $x_c$  and relative velocity of cylinder,  $U - U_c$ . Dimensionless frequency of oscillation is  $f_e/f_0 = 0.44$ .

of all vorticity concentrations. Nevertheless, in the following we consider contributions from basic classes of vortices.

For the case of a typical counter-rotating vortex pair immediately beneath the free surface, such as that shown in the upper right of image  $N = 8$  in figure 6, the effective Froude number is  $Fr = \Gamma/\pi g^{1/2}(s/2)^{3/2} = 0.28$ , the Weber number  $We =$

$2\rho\Gamma^2/\pi^2s\sigma = 0.58$ , and the Reynolds number  $Re = \Gamma/\pi\nu = 567$ . In these equations,  $\Gamma$  is circulation,  $g$  is acceleration due to gravity,  $s$  is the distance between centres of the vortices,  $\sigma$  is surface tension, and  $\nu$  is kinematic viscosity (see, for example, Dommermuth 1993 for definitions). According to the experiments of Sarpkaya & Suthon (1991), significant free-surface deformation occurs for  $Fr \geq 0.85$  (at  $We \geq 21$ ), compared with the present value of  $Fr = 0.28$  (at  $We = 0.58$ ).

For the case of a single, large-scale vortex, such as that shown in image  $N = 10$  of figure 6, the effective Froude number, following the terminology of Sarpkaya *et al.* (1994), is  $Fr = \Gamma/h(gh)^{1/2} = 0.67$ , where  $h$  is the distance from the vortex to the free surface. The corresponding value of Weber number is  $We = \rho gh^2/\sigma = 142$  and Reynolds number  $Re = \Gamma/\nu = 12637$ . In the numerical simulations of Sarpkaya *et al.* (1994), the ranges of parameters were:  $3.75 \leq Fr \leq 13.8$ ,  $0.3 \leq We \leq 30$ , and  $150 \leq Re \leq 550$ .

Finally, it should be emphasized that striations of the free surface along the span of a vortex or vortex system are not detectable using the present technique; it is anticipated that even extremely small distortions or deviations of the free surface will give rise to detectable patterns observed from this perspective.

In summary, it is remarkable that the values of circulation of the representative concentrations of vorticity described in the foregoing do not lead to significant distortions of the free surface, despite the fact they are associated with relatively large-amplitude fluctuations of the transverse force coefficient  $C_y$ , as shown in figures 1(a) and 1(b). The fact that force fluctuations can be related to the rate of change of the moments of vorticity concentrations about the cylinder is well established (Lighthill 1986) for the case of a well-submerged cylinder. Indeed, the peak-to-peak magnitudes of the  $C_y$  fluctuations for the well-submerged cylinder in figures 1(a) and 1(b) is large. The more complex origins of concentrations of vorticity from a cylinder located adjacent to the free surface and the rate of change of these patterns with time apparently provides a basis for substantial variations of  $C_y$  without inducing local distortions of the free surface. These considerations must, of course, be combined with considerations of the inviscid contribution to  $C_y$ . In the absence of viscous effects, these would involve asymmetry of the induced potential field arising from acceleration of the cylinder adjacent to an undisturbed free surface, as well as local distortions of the free surface associated with the cylinder motion. As indicated in the foregoing, however, these types of surface distortions have a very small magnitude.

## 7. Concluding remarks

This investigation has focused on a cylinder undergoing streamwise oscillations in the presence of a steady current and an adjacent free surface. The unsteady and time-averaged loading on the cylinder, as well as the formation and development of vortices in the immediate vicinity of the cylinder, are remarkably affected by proximity of the free surface. The overall aim has been to characterize the distinctive features of the cylinder loading, then to interpret them physically using patterns of instantaneous vorticity and streamline topology. Emphasis has been on the conditions of cylinder oscillations that yield locked-on states of vortex formation for the limiting case of a cylinder well-submerged beneath the free surface. The alteration of these locked-on states is addressed in relation to the degree of submergence beneath to the free surface.

In the following, the overall features of the loading on the cylinder, associated

classes of vortex formation, interpreted with patterns of vorticity and streamline topology, and corresponding free-surface signatures are briefly summarized.

### 7.1. Loading on the cylinder

Irrespective of the degree of submergence of the cylinder beneath the free surface, deterministic and repetitive signatures of the transverse  $C_y(t)$  and in-line  $C_x(t)$  force coefficients are observed over a number of cycles of the cylinder oscillation and, in some cases, for more than a hundred oscillation cycles. The signatures of  $C_y(t)$  are strongly modulated, both in amplitude and frequency; nevertheless, under certain conditions, the  $C_y(t)$  signatures are phase-locked to the cylinder motion, i.e. locked-on. Even in those cases where such phase-lock-on does not occur, the general form of the signatures is generally repeatable, at least over several cycles of the cylinder oscillation.

The degree of phase-locking has been portrayed using Lissajous representations of  $C_y(t)$  vs.  $x_c(t)$  and  $C_y(t)$  vs.  $C_x(t)$ . These portraits define regions of positive and negative hysteresis, in relation to the degree of phase-locking. As established in the previous work of Cetiner & Rockwell (2001), it is possible to attain highly repetitive phase-locked signatures of  $C_y(t)$  vs.  $x_c(t)$  for the case of the well-submerged cylinder, i.e. in the absence of free-surface effects. The present study shows, however, that when the cylinder is located close to the free surface, while maintaining a finite gap between the free surface and the surface of the cylinder such that flow occurs through the gap during a portion of the oscillation cycle, it is not possible to attain phase-locked signatures of  $C_y(t)$  over a large number of oscillation cycles of the cylinder. In other words, the effect of an adjacent free surface is a destabilizing one. In the limiting case, however, where the cylinder is located immediately beneath the free surface, such that no gap flow exists, the consequence is an opposite one. Proximity of the free surface promotes repetitive, phase-locked oscillations over a large number of oscillation cycles.

The presence of a free surface also has important consequences for the magnitude and spectral content of the  $C_y(t)$  signatures. When the oscillating cylinder is located sufficiently close to the free surface, the peak-to-peak amplitude of the  $C_y$  signature is reduced by approximately one-half. In addition, the positive peaks of the signature are attenuated dramatically in the limiting case where the cylinder is located immediately beneath the free surface; pronounced negative peaks persist, however. These alterations of the amplitude are accompanied by transformations of the time-averaged spectra of  $C_y$ . Typically, the presence of an adjacent free surface can alter the frequency of the predominant peak by as much as a factor of 4. All spectra exhibit three to four pronounced peaks, however, irrespective of the degree of submergence. In contrast to these remarkably complex, but ordered, observations of the signatures of the transverse force coefficient,  $C_y(t)$ , the in-line force coefficient  $C_x(t)$  simply exhibits phase-locked oscillations at a single predominant frequency.

All of these features described in the foregoing are linked to the time-averaged values  $\bar{C}_y$  and  $\bar{C}_x$ . When the cylinder is located immediately beneath the free surface such that no flow occurs in the gap above the cylinder, it experiences a substantial downward force. This finding is in accord with that of Miyata *et al.* (1990) for steady (non-oscillating) cylinder motion; only measurements of the averaged forces were addressed therein. A further observation is that locating the oscillating cylinder immediately beneath the free surface can dramatically lower, by nearly a factor of 2, the value of the time-averaged in-line force coefficient  $\bar{C}_x$ . The present investigation has attempted to interpret these averaged coefficients in terms of not only the unsteady

signatures  $C_y(t)$  and  $C_x(t)$ , but also to the patterns of vorticity, velocity, and streamline topology in the vicinity of the cylinder.

### 7.2. Classes of vortex formation: patterns of vorticity

As summarized in the preceding section, the signatures of  $C_y(t)$  and  $C_x(t)$  suggest either locked-on or quasi-locked-on patterns of vorticity in the near-wake region. These patterns are distinctly different from those corresponding to the classical case of Kármán vortex formation from a transversely oscillating cylinder. Moreover, they are different from the ordered patterns of vortex formation from a cylinder undergoing streamwise oscillations in the absence of free-surface effects (Cetiner & Rockwell 2001). It has been shown herein that the presence of an adjacent free surface provides the possibility for locked-on vortex formation not only from the cylinder, but also from the free surface at locations both upstream and downstream of the cylinder.

*Vortex formation from the surface of the cylinder.* In critically assessing the influence of the free surface on patterns of vortex formation, it is useful to compare the values of circulation of the classes of vortices shed from the cylinder and from the free surface. In the absence of a free surface, the large-scale clusters of vorticity formed from the lower and upper surfaces of the cylinder have dimensionless values of circulation  $\Gamma/\pi U^* D$  in the range of 1.00 to 1.16, in which  $U^*$  is the maximum value of relative velocity, i.e.  $U^* \equiv |U - U_c|_{max}$ . In the presence of a free surface, large-scale clusters of vorticity are formed from the lower surface of the cylinder. Values of  $\Gamma/\pi U^* D$  are 1.27 to 1.53 for the subharmonic oscillation and 0.68 to 1.20 for the fundamental oscillation of the cylinder. On the other hand, the existence of the free surface inhibits the circulation of vortices formed from the upper surface of the cylinder. For the case where a finite gap is maintained above the cylinder, representative values of  $\Gamma/\pi U^* D$  are 0.27 and 0.49 for excitation at the subharmonic and fundamental frequencies. In the limiting case where the cylinder is located immediately beneath the free surface, small-scale clusters of vorticity are formed from the upper region of the base rather than from the upper shoulder of the cylinder. Typical values of circulation  $\Gamma/\pi U^* D$  are 0.20 and 0.16 respectively for the subharmonic and fundamental excitation.

In addition to these types of vortex formation, which principally occur when the cylinder moves against the free stream, vortices of opposite sense can be formed from the lower and upper surfaces of the cylinder when it moves in the same direction as the free stream, provided the dimensionless frequency is sufficiently high. This type of shedding occurs for the cylinder oscillation at the fundamental frequency of Kármán vortex formation. These values of dimensionless circulation are of the order of  $\Gamma/\pi U^* D = 0.35$ .

*Vortex formation from the free surface.* Concentrations of vorticity from the free surface are consistently generated in the near wake of the cylinder. They are induced by negative (clockwise) concentrations of vorticity originally shed from the upper portion of the cylinder. These positive–negative vortices form a counter-rotating vortex pair that translates in the downstream direction along the free surface. In fact, it is possible to generate a ‘street’ of such counter-rotating pairs during a given cycle of the cylinder oscillation. The dimensionless circulation of the positive vortex formed from the free surface can be as high as  $\Gamma/\pi U^* D = 0.16$ , which is approximately one-seventh as large as the circulation of the classical Kármán vortex. These counter-rotating vortex pairs are most pronounced for the case where a finite gap exists between the free surface and the surface of the cylinder ( $h_0/D = 0.69$ ), thereby

allowing a jet-like flow, which, in turn, gives rise to a negative vortex from the surface of the cylinder; it has substantial circulation. In turn, this negative vortex induces formation of a pronounced positive vortex from the free surface. Such formation of counter-rotating vortex pairs, albeit in a modified and weaker form, is evident in the case where the cylinder is located closer to the free surface ( $h_0/D = 0.56$ ). In these cases, the vortex originates from the upper base region of the cylinder, rather than by classical shedding from the upper shoulder of the cylinder. Once these relatively weak negative vortices are formed, they induce discernible positive vorticity concentrations from the free surface.

Vortices are also formed from the free surface at locations upstream of the cylinder. In this case, however, the positive (counterclockwise) vortex is the culmination of a distributed region of vorticity extending a substantial distance upstream of the cylinder. The typical value of circulation of this vortex is  $\Gamma/\pi U^* D = 0.17$ . The generation of vorticity at the free surface is associated with the variation of tangential velocity along the surface; in some cases, it becomes part of a region of flow separation beneath the surface. The extent of this low-velocity/separated zone upstream of the cylinder can attain values as large as the cylinder diameter; in this case, the positive vorticity originally generated from the free surface eventually merges with that from the lower surface of the cylinder. Effective formation of a vortex upstream of the cylinder appears to be a strong function of the relative flow velocity. For example, maximum positive cylinder velocity corresponds to minimum relative flow velocity and, in this case, the extent of the positive vorticity concentration upstream of the cylinder shrinks. Further investigation is required in order to determine the apparent dependence on oscillation frequency of the cylinder. The most pronounced concentrations upstream of the cylinder occur at lower values of frequency, and the overall pattern is what one would expect on the basis of quasi-steady considerations, i.e. a region of substantial separated flow upstream of the cylinder. On the other hand, at the higher values of excitation frequency, these regions of vorticity upstream of the cylinder are discernible, but less pronounced, perhaps due to a favourable phase shift between the motion of the cylinder and the tendency to form a large-scale zone of flow separation.

### 7.3. Free-surface distortions

Localized distortions of a free surface due to the proximity of a vortex have been thoroughly documented, as summarized in §6. Previous investigations have primarily focused on either an isolated vortex couple, i.e. a counter-rotating vortex pair, or a single vortex. As demonstrated in the foregoing, oscillation of a cylinder beneath a free surface generates a rich array of vortical structures due to shed vorticity from both the cylinder and the free surface. It is the total vortex system that must be considered in assessing localized distortions of the free surface. Nevertheless, consideration of the dimensionless circulation of representative vortex couples and single vortices shown that the effective Froude number is substantially smaller than that typically giving rise to deformations of the free surface in the numerical and experimental studies cited in §5. This observation is in agreement with the zoomed-in measurements of the free surface in regions immediately above concentrations of vorticity. Within the spatial resolution of the present technique, no distortions are detectable. In the region immediately above the cylinder, however, small deformations of the free surface are discernible due to the cylinder motion. These distortions are of the order of  $0.034D$ .

#### 7.4. Practical significance of the major findings

The primary focus of this investigation has been on the instantaneous, global patterns of the unsteady flow and the associated instantaneous force signatures. From a practical standpoint, it is typically the time-averaged consequence of the succession of instantaneous states of the flow and forces that are of direct interest to the designer. For the types of configurations found in the field of ocean engineering, described in the first section of the Introduction, it is evident that the presence of an adjacent free surface markedly influences the time-averaged spectral content of the transverse force and the time mean values of both the transverse and in-line forces. Regarding the spectral content of the transverse force, a number of spectral peaks are present, and they extend over a relatively wide range of frequency. Onset of flow-induced vibration of an ocean structure due to unsteady loading at a defined frequency can occur in accord with the natural frequency of the structure. The present findings suggest that susceptibility to self-excited vibration is substantially enhanced by presence of multiple spectral peaks. As indicated in the foregoing, the presence of the free surface can shift the predominant spectral peak by a factor of 4 and reduce the peak spectral amplitude by as much as a factor of 2. That is, the nature of the forcing function associated with self-excited vibration is altered substantially, and the conditions for onset of vibration will be altered.

From the standpoint of steady loading, it has been demonstrated that the presence of a free surface can result in a significant downward force, i.e. a negative transverse force and, in some cases, the magnitude of the in-line force can be decreased by as much as a factor of 2.

These considerations indicate that design criteria based on the case of a fully submerged cylinder, i.e. a cylinder located at a sufficient depth beneath a free surface, will be in error by a significant margin, at least for the ranges of parameters addressed in the present investigation.

These results are relevant to the limiting case of very long-wave motion past a horizontal cylinder. In establishing the equivalence between the in-line loading addressed in the present study and that associated with actual wave motion past a cylinder, the Froude–Krylov effect (Lighthill 1986) must be accounted for.

The authors are pleased to acknowledge the primary support of the Office of Naval Research under Grant N00014-94-1-0185, P00007, monitored by Dr Thomas Swean. Supplemental support was provided by Office of Naval Research Grant N00014-99-1-0581, as well as by National Science Foundation Grant CTS-9803734, monitored by Dr Roger Arndt and Dr John Foss.

#### REFERENCES

- ANANTHAKRISHNAN, P. 1997 Three-dimensional wave-body interactions in a viscous fluid: heave oscillation of a submerged vertical cylinder. *Proc. Seventh Intl. Offshore and Polar Engineering Conference, Honolulu, USA, May 25–30*. The International Society of Offshore and Polar Engineers, ISBN 1-880653-28-1.
- ANANTHAKRISHNAN, P. & YOUNG, R. W. 1992 Oscillation of a slightly-submerged cylinder in a viscous fluid. Extended abstract for the Seventh International Workshop on Waterways and Floating Bodies, VAL de Reuil, France, May.
- BLACKBURN, H. M. & HENDERSON, R. D. 1999 A study of two-dimensional flow past an oscillating cylinder. *J. Fluid Mech.* **385**, 255–286.
- CETINER, O. N. L. 1998 Flow structure and loading due to an oscillating cylinder in steady current. PhD. Dissertation, Department of Mechanical Engineering and Mechanics, Lehigh University.

- CETINER, O. & ROCKWELL, D. 2001 Streamwise oscillations of a cylinder in a steady current. Part 1. Locked-on states of vortex formation and loading. *J. Fluid Mech.* **427**, 1–28.
- DABIRI, D. & GHARIB, M. 1997 Experimental investigation of the vorticity generation within a spilling waterwave. *J. Fluid Mech.* **330**, 113–139.
- DOMMERMUTH, D. G. 1993 Laminar interactions of a pair of vortex tubes with a free surface. *J. Fluid Mech.* **246**, 91–115.
- GHARIB, M. & WEIGAND, A. 1996 Experimental studies of vortex disconnection and connection at a free surface. *J. Fluid Mech.* **321**, 59–86.
- LIGHTHILL, J. 1986 Fundamentals concerning wave loading on off-shore structures. *J. Fluid Mech.* **173**, 667–681.
- LIN, J.-C. & ROCKWELL, D. 1999 Horizontal oscillations of a cylinder beneath a free surface: vortex formation and loading. *J. Fluid Mech.* **389**, 1–26.
- LIN, J.-C., SHERIDAN, J. & ROCKWELL, D. 1996 Near-wake of a perturbed, horizontal cylinder at a free-surface. *Phys. Fluids* **8**, 2107–2116.
- LUGT, H. J. & OHRING, S. 1992 The oblique ascent of a viscous vortex pair toward a free surface. *J. Fluid Mech.* **236**, 461–476.
- MIYATA, H. & LEE, Y.-G. 1990 Vortex motions about a horizontal cylinder in waves. *Ocean Engng* **17**, 279–305.
- MIYATA, H., SHIKAZONO, N. & KANAI, M. 1990 Forces on a circular cylinder advancing steadily beneath the free-surface. *Ocean Engng* **17**, 81–104.
- OBASAJU, E. D., BEARMAN, P. W. & GRAHAM, J. M. R. 1988 A study of forces, circulation, vortex patterns around a circular cylinder and oscillating flow. *J. Fluid Mech.* **196**, 467–494.
- OHRING, S. & LUGT, H. J. 1991 Interaction of a viscous vortex pair with a free surface. *J. Fluid Mech.* **227**, 47–70.
- OSHKAI, P. & ROCKWELL, D. 1999 Free-surface wave interaction with a horizontal cylinder. *J. Fluids Struct.* **13**, 935–954.
- ROCKWELL, D., MAGNESS, C., TOWFIGHI, J., AKIN, O. & CORCORAN, T. 1993 High image-density particle image velocimetry using laser scanning techniques. *Exps. Fluids* **14**, 181–192.
- ROOD, E. P. 1990 Interpreting vortex interactions with a free-surface. *Trans ASME I: J. Fluids Engng* **116**, 91–94.
- ROOD, E. P. 1995 Free surface vorticity. In *Free-Surface Vorticity* (ed. S. Green), Chap. 17. Kluwer.
- SARPKAYA, T. 1975 Forces on cylinders and spheres in a sinusoidally oscillating fluid. *Trans. ASME E: J. Appl. Mech.* **42**, 32–37.
- SARPKAYA, T., MAGEE, M. & MERRILL, C. 1994 Vortices, free-surface and turbulence. In *Free-Surface Turbulence* (ed. E. P. Rood & J. Katz). ASME, FED, Vol. 181, pp. 1–14.
- SARPKAYA, T. & SUTHON, P. 1991 Interaction of a vortex couple with a free surface. *Exps. Fluids* **11**, 205–217.
- SHERIDAN, J., LIN, J.-C., & ROCKWELL, D. 1997 Flow past a cylinder close to a free surface. *J. Fluid Mech.* **330**, 1–30.
- WILLIAMSON, C. H. K. 1985 Sinusoidal flow relative to a circular cylinder. *J. Fluid Mech.* **155**, 141–174.
- YU, D. & TRYGGVASSON, G. 1990 The free-surface signature of unsteady, two-dimensional vortex flows. *J. Fluid Mech.* **218**, 547–572.
- ZHU, Q., LIN, J.-C., UNAL, M. F. & ROCKWELL, D. 2000 Motion of a cylinder adjacent to a free-surface: flow patterns and loading. *Exps. Fluids* **28**, 559–575.